NASA/TM—2016-219140

Synthesis, Structure, Characterization, and Decomposition of Nickel Dithiocarbamates: Effect of Precursor Structure and Processing Conditions on Solid-State Products

Aloysius F. Hepp, Michael J. Kulis, and Jeremiah S. McNatt
Glenn Research Center, Cleveland, Ohio

Norman V. Duffy and Michael D. Hoops
Wheeling Jesuit University, Wheeling, West Virginia

Elizabeth Gorse
University of Maine, Orono, Maine

Philip E. Fanwick
Purdue University, West Lafayette, Indiana

John Masnovi
Cleveland State University, Cleveland, Ohio

Jonathan E. Cowen
Case Western Reserve University, Cleveland, Ohio

Raymond N. Dominey
University of Richmond, Richmond, Virginia

December 2016

NASA STI Program . . . in Profile

Since its founding, NASA has been dedicated to the advancement of aeronautics and space science. The NASA Scientific and Technical Information (STI) Program plays a key part in helping NASA maintain this important role.

The NASA STI Program operates under the auspices of the Agency Chief Information Officer. It collects, organizes, provides for archiving, and disseminates NASA's STI. The NASA STI Program provides access to the NASA Technical Report Server—Registered (NTRS Reg) and NASA Technical Report Server—Public (NTRS) thus providing one of the largest collections of aeronautical and space science STI in the world. Results are published in both non-NASA channels and by NASA in the NASA STI Report Series, which includes the following report types:

- TECHNICAL PUBLICATION. Reports of completed research or a major significant phase of research that present the results of NASA programs and include extensive data or theoretical analysis. Includes compilations of significant scientific and technical data and information deemed to be of continuing reference value. NASA counter-part of peer-reviewed formal professional papers, but has less stringent limitations on manuscript length and extent of graphic presentations.

- TECHNICAL MEMORANDUM. Scientific and technical findings that are preliminary or of specialized interest, e.g., "quick-release" reports, working papers, and bibliographies that contain minimal annotation. Does not contain extensive analysis.

- CONTRACTOR REPORT. Scientific and technical findings by NASA-sponsored contractors and grantees.

- CONFERENCE PUBLICATION. Collected papers from scientific and technical conferences, symposia, seminars, or other meetings sponsored or co-sponsored by NASA.

- SPECIAL PUBLICATION. Scientific, technical, or historical information from NASA programs, projects, and missions, often concerned with subjects having substantial public interest.

- TECHNICAL TRANSLATION. English-language translations of foreign scientific and technical material pertinent to NASA's mission.

For more information about the NASA STI program, see the following:

- Access the NASA STI program home page at http://www.sti.nasa.gov

- E-mail your question to help@sti.nasa.gov

- Fax your question to the NASA STI Information Desk at 757-864-6500

- Telephone the NASA STI Information Desk at 757-864-9658

- Write to:
  NASA STI Program
  Mail Stop 148
  NASA Langley Research Center
  Hampton, VA 23681-2199

NASA/TM—2016-219140

Synthesis, Structure, Characterization, and Decomposition of Nickel Dithiocarbamates: Effect of Precursor Structure and Processing Conditions on Solid-State Products

Aloysius F. Hepp, Michael J. Kulis, and Jeremiah S. McNatt
Glenn Research Center, Cleveland, Ohio

Norman V. Duffy and Michael D. Hoops
Wheeling Jesuit University, Wheeling, West Virginia

Elizabeth Gorse
University of Maine, Orono, Maine

Philip E. Fanwick
Purdue University, West Lafayette, Indiana

John Masnovi
Cleveland State University, Cleveland, Ohio

Jonathan E. Cowen
Case Western Reserve University, Cleveland, Ohio

Raymond N. Dominey
University of Richmond, Richmond, Virginia

National Aeronautics and
Space Administration

Glenn Research Center
Cleveland, Ohio 44135

December 2016

Acknowledgments

We thank the following students and collaborators for their contributions to this work: Mark Cundick (Kent State University) for synthesis of nickel dithiocarbamate complexes, Dr. Douglas Ogrin (OAI Postdoctoral Associate at NASA Glenn Research Center (GRC)) for crystal growth, Dana Anderson (NASA summer intern from University of Michigan) for assistance with pyrolysis experiments and microscopy, and Lyndsey McMillon-Brown (NASA Pathways Intern from Yale University) for assistance with X-ray powder diffraction. We are grateful to Prof. M.V.S. Chandrashekhar and colleagues from the Department of Electrical Engineering at the University of South Carolina for TEM data and analysis. Dr. James Gaier and Daniel Scheiman (NASA GRC) are acknowledged for technical discussions. Profs. Norman Duffy and Michael Hoops thank the NASA West Virginia EPSCoR program for financial support. Work at NASA Glenn Research Center was supported in part by the following programs: Internal Research and Development, Aeronautics Research Alternative Fuels, Exploration Systems Dust Mitigation, and Advanced Exploration Systems Logistics Reduction and Repurposing. Profs. Michael Hoops and John Masnovi are grateful for support through the NASA GRC Summer Faculty Fellowship Program.

Supplementary Information

The Cambridge Crystallographic Data Centre contains the full set of supplementary crystallographic data (CIFs) for this paper. These data can be obtained free of charge from The Cambridge Crystallographic Data Centre via www.ccdc.cam.ac.uk/data_request/cif (see Experimental and/or Table 1 for specific deposition numbers). More complete tables of bond lengths and angles (Tables XII to XV) are included in the Appendix.

Level of Review: This material has been technically reviewed by technical management.

Available from

NASA STI Program
Mail Stop 148
NASA Langley Research Center
Hampton, VA 23681-2199

National Technical Information Service
5285 Port Royal Road
Springfield, VA 22161
703-605-6000

This report is available in electronic form at http://www.sti.nasa.gov/ and http://ntrs.nasa.gov/

Synthesis, Structure, Characterization, and Decomposition of Nickel Dithiocarbamates: Effect of Precursor Structure and Processing Conditions on Solid-State Products

Aloysius F. Hepp, Michael J. Kulis, and Jeremiah S. McNatt
National Aeronautics and Space Administration
Glenn Research Center
Cleveland, Ohio 44135

Norman V. Duffy and Michael D. Hoops[1]
Wheeling Jesuit University
Wheeling, West Virginia 26003

Elizabeth Gorse[2]
University of Maine
Orono, Maine 04469

Philip E. Fanwick
Purdue University
West Lafayette, Indiana 47907

John Masnovi[1]
Cleveland State University
Cleveland, Ohio 44115

Jonathan E. Cowen[3]
Case Western Reserve University
Cleveland, Ohio 44106

Raymond N. Dominey
University of Richmond
Richmond, Virginia 23173

Abstract

Single-crystal X-ray structures of four nickel dithiocarbamate complexes were determined: the homoleptic mixed-organic bis-dithiocarbamates $Ni(S_2CN(isopropyl)(benzyl))_2$, $Ni(S_2CN(ethyl)(n\text{-}butyl))_2$, and $Ni(S_2CN(phenyl)(benzyl))_2$, as well as the heteroleptic mixed-ligand complex $Ni(P(phenyl)_3)(S_2CN(phenyl)(benzyl))Cl$. Synthetic, spectroscopic, structural, thermal, and materials studies are discussed in light of prior literature. The spectroscopic results are routine. A slightly distorted square-planar nickel coordination environment was observed for all four complexes. The organic residues adopt conformations to minimize steric interactions. Steric effects also may determine puckering, if any, about the nickel and nitrogen atoms, both of which are planar or nearly so. A trans-influence affects the Ni–S bond distances. Nitrogen atoms interact with the CS_2 carbons with a bond order of about 1.5, and the other substituents on nitrogen display transoid conformations. There are no strong

[1]Summer Faculty Fellow, NASA Glenn Research Center.
[2]Student Intern, NASA Glenn Research Center.
[3]NASA Graduate Student Researcher, NASA Glenn Research Center.

intermolecular interactions, consistent with prior observations of the volatility of nickel dithiocarbamate complexes. Thermogravimetric analyses of homoleptic species under inert atmosphere is consistent with production of 1:1 nickel sulfide phases. Thermolysis of nickel dithiocarbamates under flowing nitrogen produced hexagonal or α-NiS as the major phase; thermolysis under flowing forming gas produced millerite (β-NiS) at 300 °C, godlevskite (Ni_9S_8) at 325 and 350 °C, and heazlewoodite (Ni_3S_2) at 400 and 450 °C. Failure to exclude oxygen results in production of nickel oxide and sulfate (at 450 °C). Nickel sulfide phases produced seem to be primarily influenced by processing conditions, in agreement with prior literature. Nickel dithiocarbamate complexes demonstrate significant promise to serve as "single-source" precursors to nickel sulfides, a quite interesting family of materials with numerous potential applications.

Introduction

The structure and properties of metal dithiocarbamates $M(S_2CNRR')_x$ and closely related compounds (Refs. 1 to 5) remains an important topical area of research (Refs. 6 to 8). This is due not only to fundamental insights into coordination chemistry to be gained from in-depth studies of dithiocarbamates (Refs. 6 to 8), but also to their wide-ranging, practical applications in agriculture (Refs. 9 and 10), biomedicine (Refs. 10 to 12), surface science (Refs. 12 and 13), and materials science (Refs. 14 to 23). The present study is the most recent report from an ongoing effort to prepare new metal coordination compounds with sulfur-containing (i.e., thiolates or dithiocarbamates) ligands to serve as precursors for metal sulfides, most often for energy conversion (Refs. 17 and 24 to 30).

Typically, after synthesis and characterization, novel compounds have their single-crystal structures determined and their decomposition probed to assess their value as (new) "single-source" precursors for sulfide solid-state, thin-film and/or nanoparticles for possible aerospace applications. Ideally, precursors should be readily prepared from inexpensive starting materials, easily handled (preferably air stable), and/or cleanly decomposed via chemical (vapor) processing to be economically viable (Refs. 16 to 30).

The focus of this technical memorandum concerns the use of dithiocarbamates as precursors for nickel sulfide solid-state materials (Refs. 14 to 17, 19, and 21 to 23). Nickel sulfides exist in numerous stable phases (with a range of Ni:S of 3:2 to 1:2): from Ni_3S_2 (heazlewoodite) through Ni_9S_8 (godlevskite) and NiS (hexagonal (α-NiS) or rhombohedral (β-NiS or millerite)), to Ni_3S_4 (polydymite) and NiS_2 (vaesite) (Refs. 31 to 36). This report details the synthesis and characterization of three new Ni(II) unsymmetrically substituted bis-dithiocarbamates: $Ni(S_2CN(isopropyl)(benzyl))_2$ **1**, $Ni(S_2CN(ethyl)(n\text{-butyl}))_2$ **2**, and $Ni(S_2CN(phenyl)(benzyl))_2$ **3**; two symmetrically substituted (known) dithiocarbamate complexes: $Ni(S_2CN(ethyl)_2)_2$ **4** and $Ni(S_2CN(benzyl)_2)_2$ **5**; and a heteroleptic mixed-ligand complex: $Ni(P(phenyl)_3)(S_2CN(phenyl)(benzyl))Cl$ **6**.

The decomposition of five homoleptic dithiocarbamates (**1** to **5**) under anaerobic or reducing conditions at 300 to 450 °C was studied in detail. The atmosphere-dependent formation of either 1:1 NiS phases or nickel-rich sulfide phases (Ni_3S_2 or Ni_9S_8) was consistent with much of the prior literature (Refs. 14 to 17, 19, and 21). Finally, the utility of nickel dithiocarbamates as precursors to produce a variety of sulfide phases in different forms is discussed along with the potential to control product phase(s) and morphology(ies) by choice of precursor and/or processing conditions.

Experimental Details

Unless otherwise indicated, chemicals and solvents were used as received. Galbraith Laboratories, Inc. (Knoxville, TN), performed elemental analyses. All Fourier transform infrared (FTIR) spectra were the average of >100 scans collected at 2 cm^{-1} resolution from 700 to 4000 cm^{-1}.

Materials and Instruments

JASCO V-550 (University of Richmond) and Perkin-Elmer Lamba-950 model (NASA Glenn Research Center, GRC) instruments were used for electronic absorption or ultraviolet-visible (UV-vis) spectroscopy. FTIR spectra were collected on a Perkin-Elmer RX1 spectrometer (Wheeling Jesuit University, WJU), a Thermo Electron Corporation Nicolet Avatar 320 spectrometer equipped with a SensIR single-bounce Diamond 45° ZnSe thermal horizontal attenuated total reflectance (HATR) crystal (University of Richmond), or a Nicolet 380 spectrophotometer with a germanium single-pass ATR crystal (NASA GRC). A Cahn TG–2131 thermogravimetric analysis (TGA) instrument at Cleveland State University was utilized with a heating rate of 5 °C/min starting at room temperature to 800 °C under flowing nitrogen (Ref. 26). A TA Instruments SPT Q600 TGA was also utilized (WJU) as described previously that included a derivative to obtain temperature of most-rapid weight loss (Ref. 18). Initial mass loss experiments were completed at 400 °C, based upon prior studies (Refs. 14 to 17, 19, and 21 to 23).

Synthesis, Chemical Analysis, and Pyrolysis Weight Loss

Sodium *N*-R-*N*-R′-carbodithioate salts were prepared by the method of von Braun (Ref. 37) and later modified by Duffy (Refs. 38 and 39). Sodium hydroxide (6 g) was added slowly to distilled water (10 mL) cooled in an ice bath. With continued cooling, 0.10 mol of *N*-isopropyl-*N*-benzylamine, *N*-ethyl-*N*-butylamine, or *N*-phenyl-*N*-benzylamine (i.e., HN(R)(R′) with R, R′ = *i*-C_3H_7 (^{i}Pr), $CH_2C_6H_5$ (Bz); C_2H_5 (Et), *n*-C_4H_9 (^{n}Bu); or C_6H_5 (Ph), Bz; Aldrich, IR grade) was added slowly with rapid stirring, followed by reagent-grade CS_2 (6.0 mL, 0.10 mol, Fisher Scientific). After stirring and cooling for 2 h, light-brown crystals were separated and dissolved in boiling distilled water (20 mL). The mixture was cooled, and after addition of absolute ethanol (5 mL), the resulting crystals were separated by filtration, washed repeatedly with petroleum ether, air-dried overnight, and used without further purification.

Synthesis of unsymmetrical dithiocarbamates began with mixing aqueous solutions of nickel(II) chloride hexahydrate, $NiCl_2{\cdot}6H_2O$ (0.714 g, 3 mmol), and a sodium *N*-R-*N*-R′-carbodithioate salt (6 mmol). Bright green microcrystals formed immediately and were collected on a sintered-glass filter. The solid was transferred to a beaker and dissolved in $CHCl_3$ (50 mL). Any remaining aqueous fraction was discarded and the $CHCl_3$ solution was transferred to a filter flask. After addition of hexanes (50 mL), the solvent was evaporated under reduced pressure. When most of the $CHCl_3$ was removed, fine green crystals of product precipitated and were collected on a sintered-glass filter. The wet crystals were washed with hexanes until the filtrate was colorless. The compound was dried overnight; a typical yield of dithiocarbamates was ~70 percent.

A simpler synthetic method was used to prepare two symmetrically substituted compounds: bis-(di-*N*-ethyl-carbodithioato)nickel(II) **4**—$Ni(S_2CN(C_2H_5)_2)_2$, abbreviated as $Ni(dtcEt_2)_2$—which is structurally related to **2**, and bis-(di-N-benzyl-carbodithioato)nickel(II) **5**—$Ni(S_2CN(CH_2C_6H_5)_2)_2$, abbreviated as $Ni(dtcBz_2)_2$—which is structurally related to **3**. These are prepared by reacting $NiCl_2{\cdot}6H_2O$ with $Na(S_2CNEt_2)$ or $Na(S_2CNBz_2)$, respectively. Isolation and purification of the resultant products were similar to the procedure described above for compounds **1** to **3**.

Chloro(*N*-phenyl-*N*-benzylcarbodithioato)(triphenylphosphine)nickel(II) **6**—$NiP(C_6H_5)_3(S_2CN(C_6H_5)(CH_2C_6H_5))Cl$, abbreviated as $NiPPh_3$(dtcPhBz)Cl—was prepared by dissolving $Na(S_2CNPhBz)$ (0.575 g, 1.00 mmol), triphenylphosphine, PPh_3 (0.525 g, 2.0 mmol), and $NiCl_2{\cdot}6H_2O$ (0.238 g, 1.00 mmol) in boiling absolute ethanol (~20 mL). The solution was stirred at reflux for 30 min. As the solution began to cool, a fine green precipitate settled to the bottom of the beaker. The solution was filtered through a medium sintered glass filter to remove the precipitate. The red-violet solution was allowed to cool to room temperature and then cooled further in an ice bath. After 30 min, red-violet crystals formed, and *n*-heptane (10 mL) was added to further precipitate the complex. The solid was recovered by filtration through a medium sintered-glass filter, washed with *n*-heptane, and air dried overnight.

TABLE I.—ELEMENTAL ANALYSES AND PYROLYSIS WEIGHT LOSS DATA OF DITHIOCARBAMATES STUDIED

Dithiocarbamate			Powder color	Molecular weight	Analysis			
Structural formula[a]		Empirical formula			Calculated (found), percent			Mass remaining (calculated),[b] percent
					C	H	N	
1	$Ni(S_2CN^iPrBz)_2$	$C_{22}H_{28}N_2S_4Ni$	Green	507.43	52.1 (50.4)	5.6 (5.2)	5.5 (5.3)	18.4 (17.9)
2a	$Ni(S_2CNEt^nBu)_2$	$C_{14}H_{28}N_2S_4Ni$	Dk. green	411.34	40.9 (40.8)	6.9 (6.6)	6.8 (6.8)	21.2 (19.5)
3	$Ni(S_2CNPhBz)_2$	$C_{28}H_{24}N_2S_4Ni$	Green	575.47	58.4 (57.9)	4.2 (4.2)	4.9 (4.9)	15.2 (15.8)
4	$Ni(S_2CNEt_2)_2$	$C_{10}H_{20}N_2S_4Ni$	Dk. green	355.24	33.8 (34.0)	5.7 (5.7)	7.9 (7.9)	------
5	$Ni(S_2CNBz_2)_2$	$C_{30}H_{28}N_2S_4Ni$	Green	603.51	59.7 (60.6)	4.7 (4.7)	4.6 (5.0)	13.0 (15.0)
6	$NiPPh_3(S_2CNPhBz)Cl$	$C_{32}H_{27}NS_2PClNi$	Violet	614.82	62.5 (61.0)	4.4 (4.5)	2.3 (2.4)	22.0 (16.5)

[a] ^{i}Pr is *i*-C_3H_7; Bz, $CH_2C_6H_5$; Et, C_2H_5; ^{n}Bu, *n*-C_4H_9; and Ph, C_6H_5.
[b]At 400 °C; calculated for NiS.

Results of elemental analyses and pyrolysis weight loss (except for **4**, vide infra) are reported in Table I. The most likely cause of the low carbon analyses for **1** and **6** is precipitation of unreacted $NiCl_2 \cdot 6H_2O$ along with the dithiocarbamate complexes. Given the goals of this study and satisfactory confirmation from other characterization methods, further purification was not attempted.

X-Ray Crystallography

Microcrystals of each compound were dissolved in hot ethanol, and single crystals suitable for X-ray diffraction (XRD) grew by slow evaporation of the solvent upon standing for three weeks at room temperature. Crystals of **1** were dark green equant, **2a** were dichroic orange prismatic, **3** were dichroic green prismatic, and **6** were violet prismatic. Single crystals were cemented to a quartz fiber with epoxy glue in a random orientation. X-ray intensity data were collected at 150 K on a Nonius Kappa CCD X-ray diffractometer system using graphite monochromated Mo K_α radiation (λ = 0.71073 Å).

Refinement was performed on a Digital Equipment Corporation AlphaServer 2100 using SHELX-97 (Ref. 40). Cell constants for data collection were obtained from least-squares refinement and the space groups were determined using the program XPREP (Ref. 40). Frames were integrated with DENZO-SMN (Ref. 41). Lorentz and polarization corrections were applied to the data. Structures were solved using the program PATTY in DIRDIF-99 (Ref. 42) for compounds 1, 2a, and 6 and by direct methods using SIR-2004 (Ref. 43) for compound **3**. Scattering factors were taken from the International Tables for Crystallography (Ref. 44). Crystallographic drawings were produced using ORTEP (Ref. 45) and PLUTO (Ref. 46).

The crystallographic information is summarized in Table II. ORTEPs showing the atom labeling schemes are given in Figures 1 to 4 and cell diagrams are shown in Figure 5. Deposition numbers for crystallographic information files deposited with the Cambridge Crystallographic Data Centre are given in Table II.

Nickel Dithiocarbamate Thermolysis and Pyrolysate Characterization

For thermolyses, compounds **1** to **5** were packed into alumina boats and heated in a tube furnace with flowing (150 cm^3/min or sccm) nitrogen or forming gas (4% H_2 in Argon (Ar)) at 300 to 450 °C for an hour. The pyrolysis temperature was chosen based upon data from TGA experiments showing significant weight loss and essentially complete decomposition at temperatures below 400 °C. Flowing nitrogen provided an inert atmosphere to preclude interaction with oxygen; forming gas provided for further reaction and removal of sulfur. Scanning electron microscopy demonstrated production of nanocrystals from microcrystalline dithiocarbamates, and XRD (powder) of pyrolysates identified major phases of (nano)crystalline materials.

Scanning electron microscopy was performed on a Hitachi 3000 instrument at NASA GRC, transmission electron microscopy (TEM) on a Hitachi H8000 at the Electron Microscopy Center at the University of South Carolina. Powder XRD was performed on a PANalytical X'pert Pro system (NASA GRC). Thermolysis was accomplished using a sealed tube furnace under flowing nitrogen or forming gas (4 percent hydrogen in argon) at NASA GRC; this is a simplified version of a system described previously (Ref. 18).

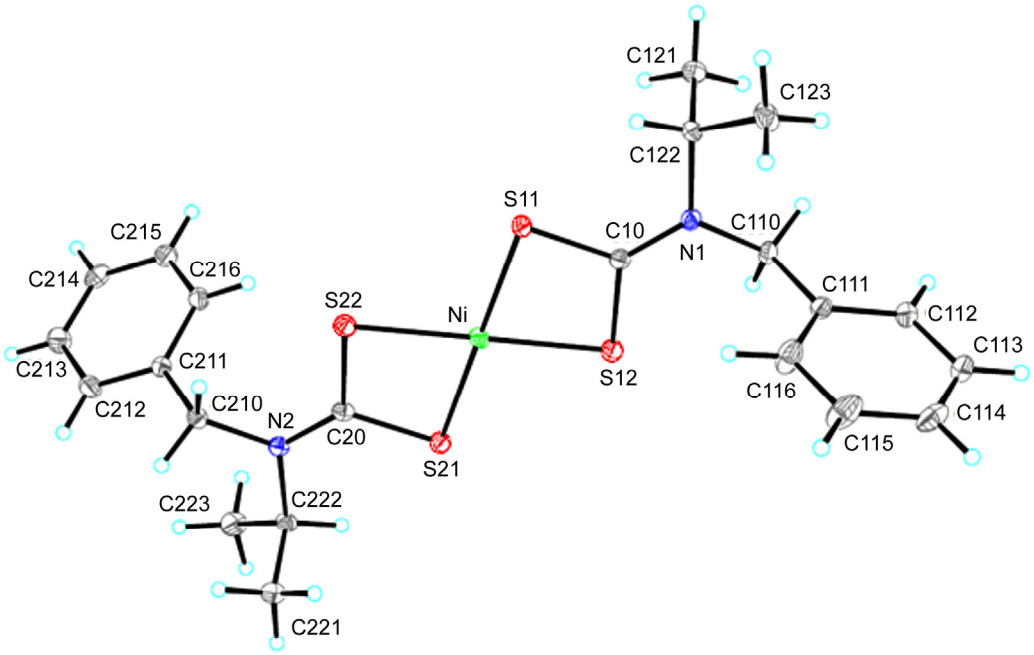

Figure 1.—ORTEP (Ref. 45) diagram with 30 percent thermal ellipsoids and atomic labeling scheme of synthesized dithiocarbamate $Ni(S_2CN(isopropyl)(benzyl))_2$ **1**.

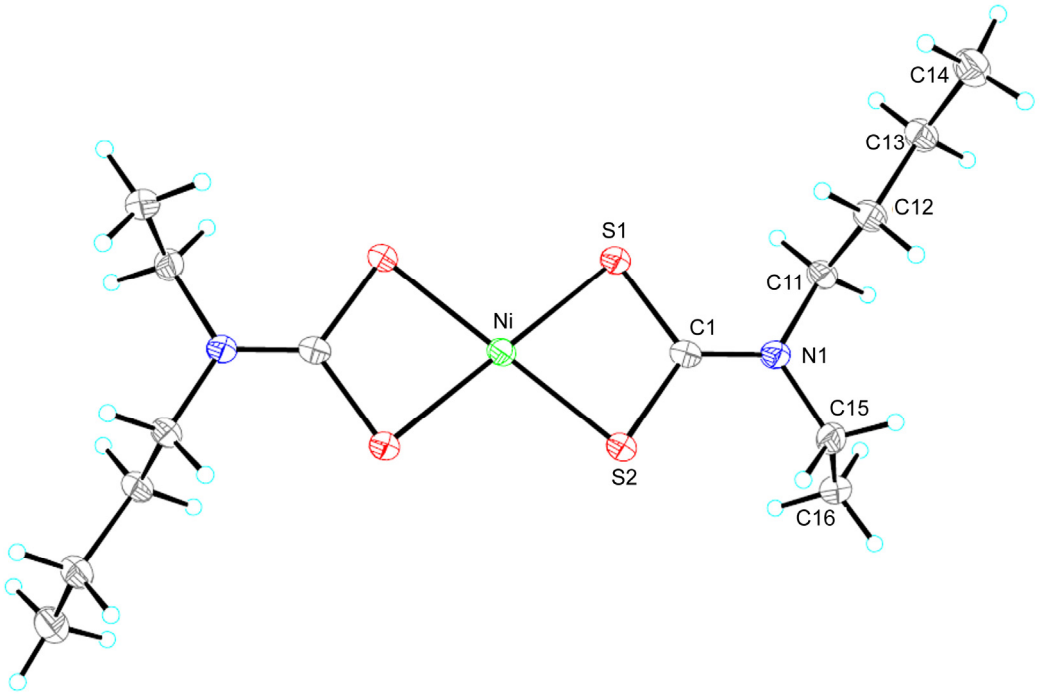

Figure 2.—ORTEP (Ref. 45) diagram with 30 percent thermal ellipsoids and atomic labeling scheme of synthesized dithiocarbamate $Ni(S_2CN(ethyl)(n\text{-}butyl))_2$ **2a**.

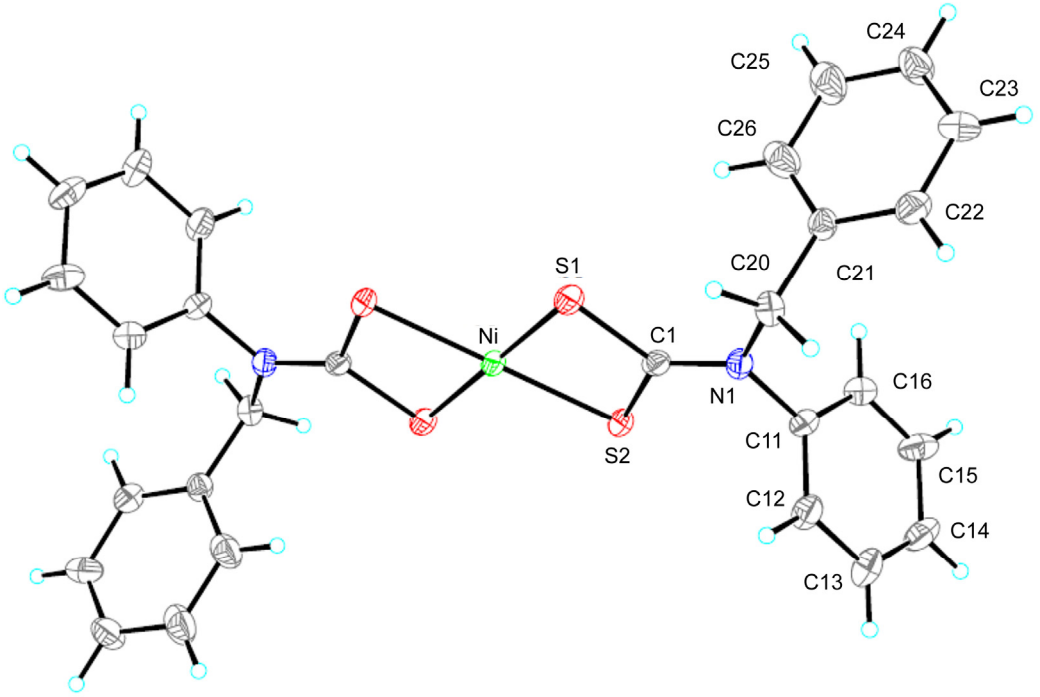

Figure 3.—ORTEP (Ref. 45) diagram with 30 percent thermal ellipsoids and atomic labeling scheme of synthesized dithiocarbamate $Ni(S_2CN(phenyl)(benzyl))_2$ **3**.

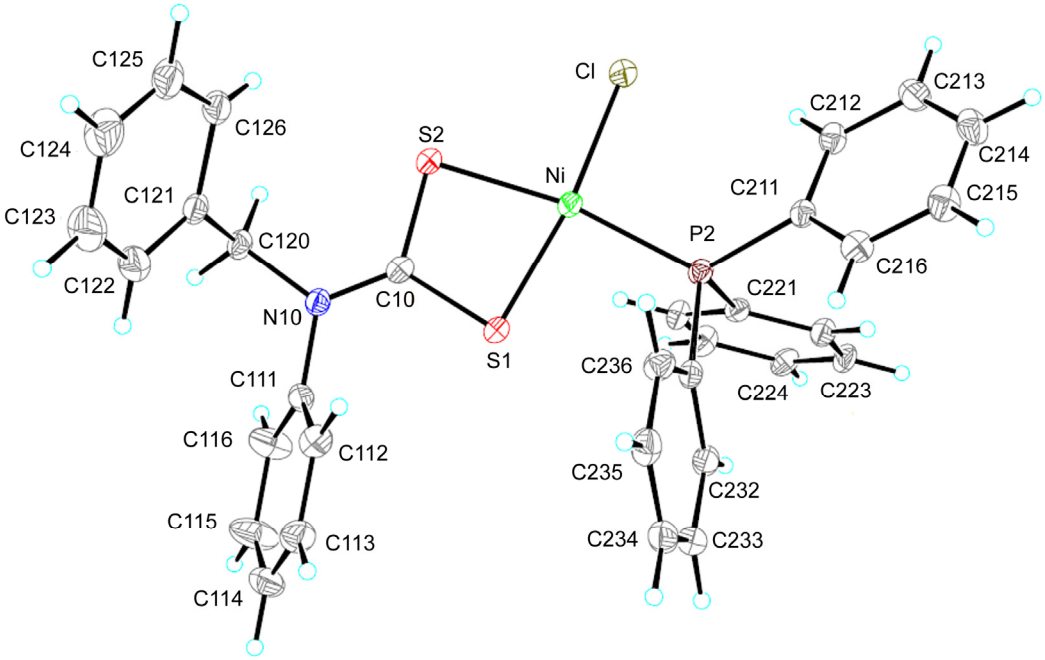

Figure 4.—ORTEP (Ref. 45) diagram with 30 percent thermal ellipsoids and atomic labeling scheme of synthesized dithiocarbamate $Ni(P(phenyl)_3)(S_2CN(phenyl)(benzyl))Cl$ **6**.

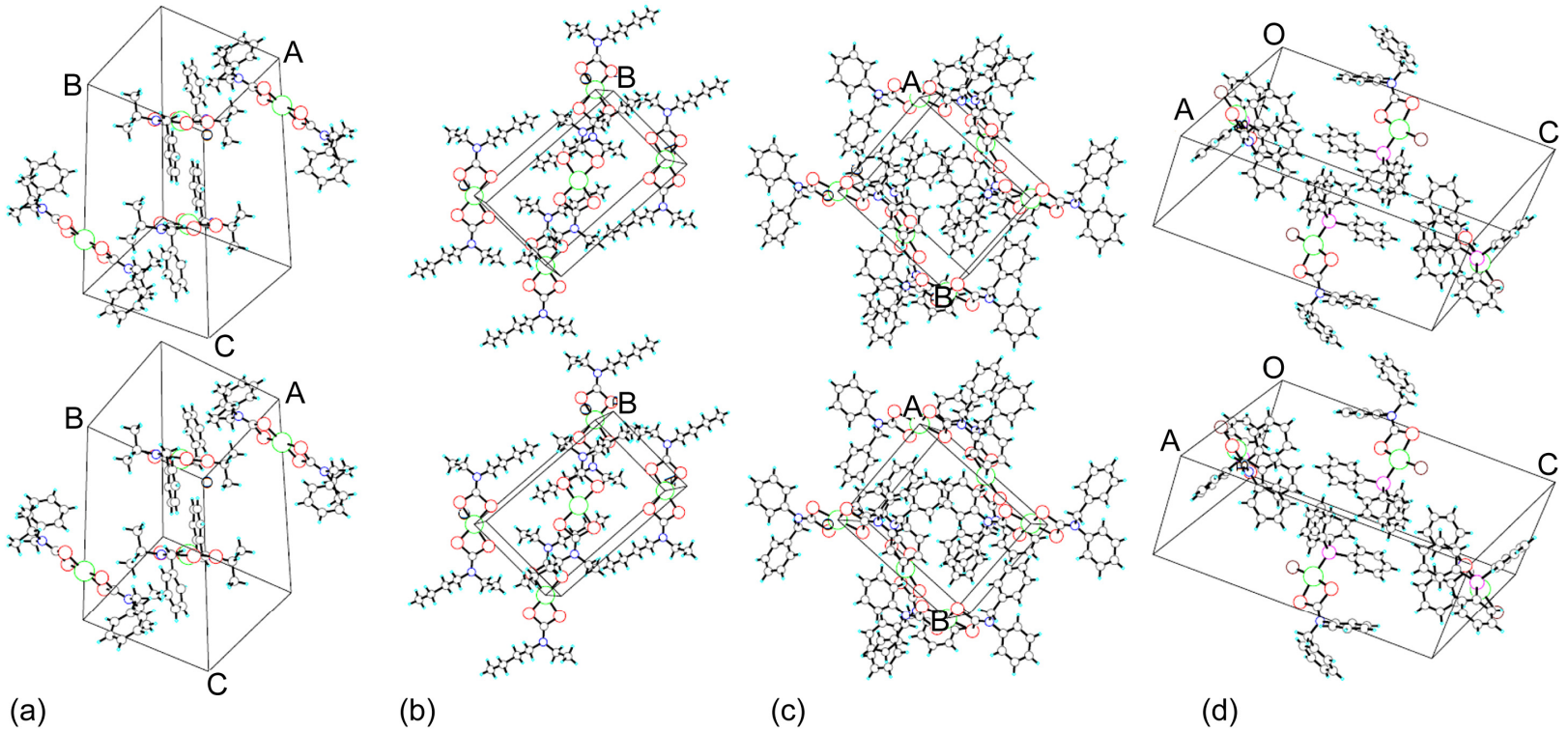

Figure 5.—Cell diagram stereoviews of synthesized dithiocarbamates. Nickel is represented by green circles; sulfur, by red; phosphorus, by magenta; carbon, by gray; nitrogen, by blue; and hydrogen, by cyan. (a) $Ni(S_2CN(isopropyl)(benzyl))_2$ **1**. (b) $Ni(S_2CN(ethyl)(n\text{-}butyl))_2$ **2a**. (c) $Ni(S_2CN(phenyl)(benzyl))_2$ **3**. (d) $Ni(P(phenyl)_3)(S_2CN(phenyl)(benzyl))Cl$ **6**.

TABLE II.—SUMMARY OF CRYSTALLOGRAPHIC DATA FOR COMPOUNDS **1**, **2a**, **3**, AND **6**

Data	Compound			
	1	**2a**	**3**	**6**
Empirical formula	$C_{22}H_{28}N_2NiS_4$	$C_{14}H_{28}N_2NiS_4$	$C_{28}H_{24}N_2NiS_4$	$C_{32}H_{27}ClNNiPS_2$
Molecular weight	507.43	411.34	575.46	614.82
Crystal system	Monoclinic	Monoclinic	Monoclinic	Monoclinic
Space group	$P2_1/n$ (No. 14)	$P2_1/n$ (No. 14)	$P2_1/c$ (No. 14)	$P2_1/n$ (No. 14)
Crystal data				
Lattice parameters				
a, Å	10.5407(2)	8.4442(5)	10.0329(6)	13.9479(3)
b, Å	11.1598(2)	8.4633(6)	11.7342(7)	9.7908(3)
c, Å	19.9164(5)	13.5293(9)	11.4362(4)	22.4583(7)
α, deg	90	90	90	90
β, deg	92.3629(8)	94.626(4)	92.709(8)	107.7183(12)
γ, deg	90	90	90	90
Unit cell parameters				
Volume, V, Å^3	2340.82(8)	963.73(11)	1344.86(12)	2921.45(14)
Z	4	2	2	4
Density, D_{calc}, g·cm^{-3}	1.440	1.417	1.421	1.398
Absorption coeff., μ, mm^{-1}	1.186	1.423	1.042	0.972
Structure factor,[a] $F(000)$	1064	436	596	1272
Crystal size, mm	0.30×0.30×0.30	0.30×0.30×0.18	0.44×0.35×0.28	0.44×0.35×0.31
Temperature, K	150	150	150	150
θ range collected, deg	2.05 to 27.48	2.41 to 27.47	2.49 to 27.50	2.04 to 27.48
Data collected	17437	7118	18305	20715
Unique data (R_{int})	5297 (0.027)	2161 (0.029)	3024 (0.037)	6653 (0.048)
Transmission factors, T_{max}, T_{min}	0.70, 0.61	0.77, 0.67	0.75, 0.67	0.74, 0.65
Data with $I > 2.0\sigma(I)$	4106	1682	2394	4428
Data refinement				
$R(F_o)$[b]	0.035	0.037	0.030	0.045
$wR(F_o^2)$[c]	0.080	0.100	0.072	0.106
Largest difference peak and hole, e Å^{-3}	0.37, –0.65	0.58, –0.72	0.36, –0.32	0.66, –0.58
Goodness of fit (GOF) on F^2	0.993	1.020	1.071	1.025
CCDC deposit number[d]	761180	761181	601390	761182

[a] Non-dispersive $F(000)$ is a positive number and counts the effective number of electrons in the unit cell.

[b] $R = \sum \left| |F_o| - |F_c| \right| / \sum |F_o|$ for $F_o^2 > 2\sigma(F_o^2)$.

[c] $wR = \left[\sum w\left(|F_o| - |F_c|\right)^2 / \sum w\left(|F_o^2|\right)^2 \right]^{1/2}$.

[d] CCDC is the Cambridge Crystallographic Data Centre.

Analysis and Characterization

Spectral analysis of the four unsymmetrically substituted complexes is summarized in Table III. Electronic absorption (UV-vis) spectra were determined from saturated cyclohexane (250 to 550 nm) or 3 mmol chloroform (450 to 800 nm) solutions of compounds **1** to **3** and **6**. Also listed in Table III are infrared spectral data from two of the three most often-studied regions (Refs. 1 to 5 and 51) near energies determined (Ref. 52) for C···S (1000±50 cm^{-1}) and C···N ("thiureide" 1500±50 cm^{-1}) dithiocarbamate bonds. Selected bond lengths and bond angles for compounds **1**, **2**, **3**, and **6** are given in Table IV.

TABLE III—SPECTRAL DATA FOR
NICKEL DITHIOCARBAMATE COMPLEXES
(**1** TO **3** AND **6**)

Compound[a]	Infrared bands, cm^{-1}		UV-visible bands	
	Spectral region			
	ν(C⋯S) 950–1050	ν(C⋯N) 1450–1550	$cm^{-1}\times10^3$	nm
$Ni(S_2CN^iPrBz)_2$ **1**	1030w ~980(sh) 962m	~1495(sh) 1478vs 1450m	15.9 20.4(sh) 25.1 30.5 40.3 47.6	630 490 398 328 248 215
$Ni(S_2CNEt^nBu)_2$ **2a**	1035w 1015w 993m 954m	1538m 1507s 1464m	15.9 20.4(sh) 25.5 30.7 40.3 46.5(sh)	630 490 392 326 248 215
$Ni(S_2CNPhBz)_2$ **3**	1030m 999w 975w 950m	1487s 1467s 1450m	15.9 20.4(sh) 23.8 30.3 39.7 47.6	630 490 420 330 252 210
$Ni(PPh_3)(S_2CNPhBz)Cl$ **6**	1028w 995m 970w	1494(sh) 1482m 1450w	19.2 24.0 29.9 39.7 46.5(sh)	520 416 334 252 215

[a]Pr is isopropyl, Bz is benzyl, Et is ethyl, Bu is butyl, and Ph is phenyl.

TABLE IV.—SELECTED AVERAGE BOND LENGTHS (Å) AND ANGLES (°)
IN COMPOUNDS **1**, **2**, **3**, AND **6**

Bond	**1**	**2a**	**2b**	**3**	**6**
Length,[a] Å					
Ni−S	2.2040	2.2082	2.2033	2.2020	2.1878(8)[b]
----------	--------	--------	--------	--------	2.2342(8)[c]
S−C	1.7235	1.720(2)	1.714	1.7194	1.718
N−CS_2	1.3185	1.321(3)	1.319(3)	1.318	1.313(4)
N−Ph	1.4725	--------	--------	1.445	1.456(4)
N−CH	1.492	1.471	1.4735	1.475	1.478(3)
Alkyl C−C	1.5205	1.521	1.5095	--------	--------
C−Ph	1.5135	--------	--------	1.509(2)	1.510(4)
Ni−Cl	--------	--------	--------	--------	2.18000(8)
Ni−P	--------	--------	--------	--------	2.2010(8)
Angle,[a] deg					
Bond	**1**	**2a**	**2b**	**3**	**6**
S−Ni−S	79.281	79.28(2)	79.18	79.55(1)	78.31(3)
----------	100.71	100.72(2)	100.82	100.45(1)	----------
----------	178.75	180.00	180.0	180.0	----------
Ni−S−C	85.555	85.42	85.40	85.20	86.48
C−N−CS_2	120.28	121.44	121.55	121.15	121.1
C−N−C	118.54	117.1(2)	117.48	117.5(1)	117.8(2)
S−C−S	109.34	109.87(15)	110.04	110.04(9)	108.71(16)
S−C−N	125.33	125.06	124.95	125.0	125.65

[a]Values reported with standard deviations are unique.
[b]S1 (trans to Cl).
[c]S2 (trans to P).

Spectroscopic Analysis

For compounds **1** to **3** with square-planar d^8 NiS_4 configurations, two low-energy weak ($\varepsilon \leq 200$) absorptions at 630 and 490 nm have been attributed to d-d bands (Refs. 47 and 48). The next higher energy absorption at 392 to 420 nm, has been assigned to a metal-to-ligand charge transfer (MLCT, or $d \rightarrow L\pi^*$) band (Refs. 47 and 48). The three intense high-energy bands arise from intraligand transitions of the coordinated dithiocarbamates and/or ligand-to-metal charge transfer (LMCT) bands (Refs. 47 to 49). For compound **6** the lowest energy band is assigned to a d-d band, the band at 416 nm to a triphenylphosphine LMCT band, and the three intense UV bands as above to intraligand or LMCT transitions (Ref. 50).

While the number and energies of C···S and C···N infrared bands serve as one simple guide (after Bonati and Ugo (Ref. 53)) to determining coordination mode of dithiocarbamate ligands (chelating vs. monodentate), it is no longer thought to be an ideal heuristic for determining the coordination modes of dithiocarbamate complexes, especially for solid-state spectra, owing to symmetry considerations, and more complicated *N*-substituents (Refs. 5 and 51) that contribute a C–N stretch in the range of 1020 to 1090 cm^{-1}. The potential for combination bands and/or Fermi resonance from this band as well as the fundamental (aromatic ring stretch, 1450 to 1510 cm^{-1}) and overtone (first overtone of C–H out-of-plane bending for monosubstituted aromatic rings, 730 to 770 cm^{-1}) vibrations involving aromatic moieties of the dithiocarbamate ligands, for example, may further complicate the analysis and may account for the slightly lower stretching frequency and multiple strong peaks in the thiureide region of the FTIR spectra of compounds **1**, **3**, and **6** (Ref. 54).

All four unsymmetrically substituted complexes have bands of medium intensity in the region of 730 to 745 cm^{-1}. The first overtone of this band would be between 1460 to 1490 cm^{-1}, in fact there is a band in this energy region observed for all four complexes. In the case of compound **2**, the peak at ~1460 cm^{-1}, could be assigned to a first overtone of a $-(CH_2)_n-$ methylene rocking band for $n \geq 3$ (720 to 750 cm^{-1}) as would be expected for a ^{n}Bu-containing ligand and/or a methylene C–H bend fundamental band (1445 to 1485 cm^{-1}) (Ref. 54). Prior reviews and more detailed prior literature on this topic should be consulted for more in-depth discussion(s) (Refs. 1 to 5 and 51 to 55).

X-Ray Structural Characterization and Analysis

Structural determinations for the four complexes (Table IV) allow for a comparison to the abundant literature for structures of dithiocarbamate complexes related to both homoleptic (**1** to **3**) (Refs. 5, 19, 22, and 56 to 62) and heteroleptic (**6**) (Refs. 63 to 65) compounds of this study (Table V). A structure determination for $Ni(S_2CNEt^nBu)_2$ (**2b**) has been reported previously (Ref. 60) with a different unit cell than our data (**2a**) although in the same space group and is included here for comparison. The asymmetric units of compounds **2a** and **3** comprise one-half of these molecules with the metal atoms lying on inversion centers. As expected, the phenyl groups in compounds **1**, **3**, and **6** are essentially planar. The butyl chain in **2a** adopts an all-anti conformation, and the butyl and ethyl chains also are directed to opposite sides of the core structure; this should be the lowest energy conformation, minimizing steric interactions. The nickel atoms necessarily reside in the plane of the ligands in **2a** and **3** due to the symmetry, but they pucker slightly to lie above this plane by 0.0212(3) Å in **1** and 0.0446(5) Å in **6**.

The average Ni–S bond lengths for the three homoleptic (2.2020(5) to 2.2084(6) Å) and the mixed-ligand **6** (2.2110(8) Å) complexes are unexceptional. Of the three homoleptic species, the bis-isopropylbenzyl complex (**1**) is the most asymmetric with a difference in Ni−S bond lengths of 0.0118(5) Å, similar to several other homoleptic unsymmetrical complexes involving mixed (aryl-alkyl or proton-alkyl) substituents (R-R′ = ^{n}Bu-Bz, H-Pr, H-adamantyl, methyl-Ph) (Refs. 22, and 57 to 59). The unsymmetrically substituted compounds (**2a** and **3**) with either two aliphatic or aromatic substituents have nearly symmetrical Ni–S coordination, typical of other nickel dithiocarbamates (Refs. 5, 19, 56, and 60 to 62).

TABLE V.—AVERAGE BOND DISTANCES AND ANGLES FOR UNSYMMETRICAL Ni DITHIOCARBAMATE COMPLEXES[a,b]

Compound[c]	Ni–S, Å	S–Ni–S, Deg	S···C, Å	S–C–S, deg	Ni–S–C, deg	C···N, Å	C–N, Å	Text (Ref.)/ (**Compound**)
$Ni(S_2CN(H)Me)_2$	2.200	79.2	1.71	109.8	-----	1.30	1.47	(Ref. 56)
$Ni(S_2CN(H)Pr)_2$	2.198	79.92	1.715	110.7	84.5	1.295	1.455	(Ref. 57)
$Ni(S_2CN(H)Adm)_2$[d]	2.201	79.12	1.725	108.69	86.05	1.314	1.473	(Ref. 58)
$Ni(S_2CNMe^nBu)_2$	2.203	79.20	1.716	109.8	-----	1.315	-----	(Ref. 19)
$Ni(S_2CNMePh)_2$	2.203	79.3	1.72	109.3	85.6	1.30	1.48	(Ref. 59)
$Ni(S_2CNEt^nBu)_2$	2.2033	79.18	1.714	110.04	85.40	1.319	1.481	(Ref. 60)/**(2b)**
$Ni(S_2CNEt^nBu)_2$[e]	2.2084	79.28	1.722	109.9	85.42	1.321	1.471	**(2a)**
$Ni(S_2CNEtCy)_2$[f]	2.1967	79.58	1.724	109.3	85.57	1.314	1.484	(Ref. 61)
$Ni(S_2CN^iPrBz)_2$[e]	2.2040	79.29	1.724	109.4	85.69	1.319	1.482	**(1)**
$Ni(S_2CN^nBuBz)_2$[d]	2.2041	79.20	1.715	109.9	85.4	1.322	1.482	(Ref. 22)
$Ni(S_2CNCH_2C_4H_3NBz)_2$	2.205	79.48	1.731	109.0	85.8	1.292	1.487	(Ref. 62)
$Ni(S_2CNPhBz)_2$[e]	2.2020	79.55	1.720	110.04	85.20	1.318	1.460	**(3)**
$Ni(PPh_3)(S_2CN^iPrBz)Cl$	2.215(3)[h] 2.176(3)	78.83(12)	1.718	108.4(6)	86.3	1.326(14)	1.485	(Ref. 63)
$Ni(PPh_3)(S_2CN^nBuBz)Cl$[g]	2.2224(11)[h] 2.1745(11)	79.02(3)	1.730	107.93(11)	86.53	1.309(3)	1.471	(Ref. 64)
$Ni(PPh_3)(S_2CNPhBz)Cl$[e]	2.2342(8)[h] 2.1878(8)	78.31(12)	1.718	108.7(1)	86.5	1.313(4)	1.467	**(6)**
$Ni(PPh_3)(S_2CN^iPrBz)Br$	2.2205(8)[h] 2.1851(8)	78.05(3)	1.716	107.9(2)	87.0	1.316(4)	1.487	(Ref. 63)
$Ni(PPh_3)(S_2CN(H)Ph)Br$[g]	2.2128(16)[h] 2.1814(16)	78.38(6)	1.713	108.3(3)	86.3	1.329(8)	1.436	(Ref. 65)
$Ni(PPh_3)(S_2CN^iPrBz)I$	2.2087(12)[h] 2.1882(12)	79.13(5)	1.717	107.7(2)	87.1	1.325(4)	1.477	(Ref. 63)

[a]Values with standard deviations are unique.
[b]Temperature of data collection 293±2 K unless otherwise specified.
[c]Adm is adamantyl; Cy is cyclohexyl.
[d]Temperature of data collection 120 K.
[e]Temperature of data collection 150 K.
[f]Temperature of data collection 200 K.
[g]Temperature of data collection 100 K.
[h]Bond trans to phosphorus.

The Ni−S bonding in compound **6** and analogous complexes (Refs. 63 to 65) is quite asymmetric, however, with the Ni−S(1) bond trans to the electron-withdrawing chloride being shorter than the Ni–S bond trans to the phosphine by 0.0464(8) Å. This asymmetry has been observed previously for structurally related neutral compounds including symmetrically substituted heterocyclic complexes $Ni(PPh_3)(S_2CNRR')(X)$, R,R′ = Et, ″Bu, $(CH_2)_4$; X = Cl, Br, I, NCS (Refs. 66 to 68). It can be ascribed to a structural trans-effect, phosphines being stronger trans-influencing ligands than chloride as found commonly in square planar complexes of the other metals in the same family (Pd and Pt) (Ref. 69).

Bond lengths involving the sp^2 hybridized carbons (C1 or C10) near the core of the dithiocarbamate complexes are typically 1.71(1) to 1.73(2) Å for S···C and 1.29(1) to 1.33(1) Å for N···C, consistent with a number of previously reported homoleptic and heteroleptic complexes (Refs. 5, 19, 22, and 56 to 68). As expected, the N−C(sp^3) single bonds attached to the organic substituents are longer by ~0.15 Å than the N−CS_2 bond and are typical (1.47±0.02 Å) for all four complexes (Ref. 5). Bond lengths near 1.3 Å found for the N−CS_2 bonds are more characteristic of N=C double bonds (Ref. 70) and indicate considerable double bond character to be present between N and the CS_2 carbon in these complexes (Ref. 58).

A hybridization of sp^2 also is consistent with the observation of small pyramidalization of the nitrogens, which are nearly planar in **2a** and **3** (Table VI). The effect would be to shift electron density from nitrogen to sulfur, placing the nickel atom in a relatively electron-rich environment. The greatest pyramidalization is found in **1**, due possibly in part to the steric demands of the isopropyl group. However, since the nitrogens in **3** and **6** are similarly substituted yet pyramidalize to different degrees, other effects such as molecular packing likely contribute as well. Small pyramidalization about nitrogen is

TABLE VI.—DISTANCES (Å) OF ATOMS FROM THE SPECIFIED PLANES

Compound	Ni from ligands	$C(S_2)$ from ligands	N from attached C
1 $Ni(S_2CN^iPrBz)_2$	0.0212(3)	0.0221(19), 0.045(2)	0.081(2), 0.0763(19)
2a $Ni(S_2CNEt^nBu)_2$	0	0.020(3)	0.016(2)
2b $Ni(S_2CNEt^nBu)_2$[a]	0	0.007(3)	0.009(3)
3 $Ni(S_2CNPhBz)_2$	0	0.011(2)	0.0367(16)
6 $Ni(PPh_3)(S_2CNPhBz)Cl$	0.0446(5)	0.004(3)	0.004(3)

[a]Coordinates from Reference 60.

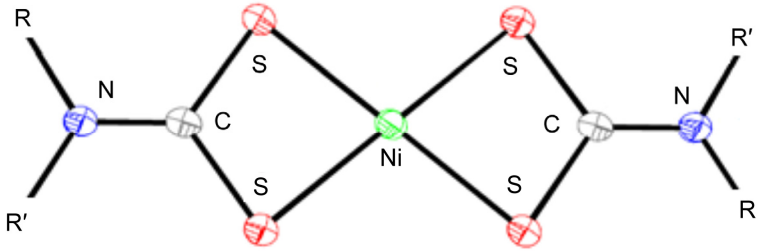

Figure 6.—Transoid orientation of the alky groups (R,R′) in synthesized dithiocarbamates $Ni(S_2CN(isopropyl)(benzyl))_2$ **1**, $Ni(S_2CN(ethyl)(n\text{-}butyl))_2$ **2a**, $Ni(S_2CN(phenyl)(benzyl))_2$ **3**, and (d) $Ni(P(phenyl)_3)(S_2CN(phenyl)(benzyl))Cl$ **6**.

common in sp^2-hybridized aromatic amines such as carbazoles and occurs with little sacrifice of energy (Ref. 71). Since the nitrogen atoms are nearly planar and lie close to the plane of the inorganic core atoms, cisoid and transoid conformations are possible for the two alkyl or aryl substituents R,R′ on nitrogen in the homoleptic derivatives **1** to **3**. The transoid geometry, in which the same organic groups are located on opposite sides of the structure, is found for all three (Fig. 6). This orientation should minimize steric interactions and is expected to be lowest in energy.

The chelated S−Ni−S bond angle for the three homoleptic compounds are similar (79.28(2) to 79.55(2)°), typical for homoleptic complexes reported in the literature which average 79.5±0.4° (Refs. 5, 19, 22, and 56 to 62). The heteroleptic compound **6** has a smaller bite of 78.31(12)°, within the margin of error for related mixed-ligand triphenylphosphine dithiocarbamate (pseudo)halide complexes, with an average bond angle of 78.7±0.4° (Refs. 63 to 68). The S−C−S bond angle of 110.04° for **3** is similar to that of **1** and **2a** and is typical for asymmetrically substituted homoleptic compounds (Refs. 5, 19, 22, and 56 to 62). This angle is more than 1° smaller in **6**, which like **3** also bears benzyl and phenyl organic residues, and corresponds to an S−Ni−S angle that is smaller by about the same amount, consistent with observations for other heteroleptic compounds (Refs. 63 to 68). The smaller bite angles about nickel and carbon in compound **6** are probably once again attributable to steric effects, here involving the five phenyl groups.

The Ni−S−C bond angles for **1** to **3** of 85.20(6) to 85.68(7)° are in the midrange of 85.5±0.5° observed for other homoleptic compounds (Refs. 5, 19, 22, and 56 to 62), and the slightly wider angle found in **6** of 86.5(1)° is typical of the heteroleptic species (Refs. 63 to 68). Slight differences in the shape of the central ring of the two types of compounds could be a result of the effect of electron withdrawing (pseudo-)halides. Bond lengths and angles outside of the core ring structure vary considerably as there are a large number of structural types; more overarching analyses of bonding-structure correlations in dithiocarbamates and related complexes as well as potential correlations to spectroscopy have been addressed previously (Refs. 1 to 5).

The structures reveal only weak intermolecular interactions. Putative weak intermolecular hydrogen bonds to sulfur with S···H′ distances less than the sum of the van der Waals radii (3.0 Å) are found in **1**, **2a**, and **6**, whereas the interactions in **3** occur just beyond this distance (Table VII). The closest contacts are found in **1** (2.824 Å) and in **2a** (2.631 Å), indicating that steric effects involving the phenyl groups likely prevent as close an approach to the core ring in **3** and **6**. Two additional weak hydrogen bonds involving Cl also are present in **6** with Cl···H′ distances near the sum of the van der Waals radii (2.95 Å).

TABLE VII.—NONBONDED INTRAMOLECULAR AND INTERMOLECULAR DISTANCES AND ANGLES[a]

Atomic interaction	Distance, Å	Atomic interactions	Angle, deg	Atomic interactions	Angle, deg	Atomic interactions	Angle, deg
Ni(S$_2$CN(isopropyl)(benzyl))$_2$ **1**							
Ni---H214	3.008						
S11···H113′	3.022	C10–S11···H113′	145.1	Ni–S11···H113′	89.0	S11···H113′–C113′	147.4
S12···H213′	2.824	C10–S12···H213′	166.7	Ni–S12···H213′	104.6	S12···H213′–C213′	148.5
C223···C223′	3.390(4)						
Ni(S$_2$CN(ethyl)(*n*-butyl))$_2$ **2a**							
Ni---H14C	3.454						
S1···H16B′	2.847	C1–S1···H16B′	173.8	Ni–S1···H16B′	98.0	S1···H16B′–C16′	101.0
S2···H15A′	2.631	C1–S2···H15A′	159.4	Ni–S2···H15A′	151.6	S2···H15A′–C15′	107.5
Ni(S$_2$CN(phenyl)(benzyl))$_2$ **3**							
Ni---H24	3.157						
S1···H12′	3.019	C1–S1···H12′	134.7	Ni–S1···H12′	92.0	S1···H12′–C12′	132.9
S1···H23′	3.018	C1–S1···H23′	91.7	Ni–S1···H23′	111.8	S1···H23′–C23′	155.7
S2···H20A′	3.014	C1–S2···H20A′	96.2	Ni–S2···H20A′	114.5	S2···H20A′–C20′	127.3
NiP(phenyl)$_3$(S$_2$CN(phenyl)(benzyl))Cl **6**							
Ni---H215	3.327						
Cl···H116′	2.958	Ni–Cl···H116′	94.0	Cl···H116′–C116′	147.2		
Cl···H123′	2.901	Ni–Cl···H123′	164.0	Cl···H123′–C123′	165.9		
S2···H116′	2.956	C10–S2···H116′	60.0	Ni–S2···H116′	92.9	S2···H116′–C116′	145.0
S2···H215′	2.891	C10–S2···H215′	88.5	Ni–S2···H215′	79.8	S2···H215′–C215′	141.2
C114···H212′	2.972						
C214···H233′	2.975						

[a]Dashed lines represent intramolecular interactions, dotted lines intermolecular interactions, and primed atoms represent positions in a different molecule. van der Waals contact distances: CH 2.90, CC 3.40, SH 3.00, ClH 2.95, NiH 2.83; see http://periodictable.com/Properties/A/VanDerWaalsRadius.al.html.

The interaction diagrams in Figure 7 indicate that the nickel atoms have no close intermolecular contacts despite the coordination being essentially planar. Instead, the organic moieties of adjacent molecules fit hand-in-glove in the region about the open axial coordination sites. Steric effects arising from the organic groups would be present here as well, and in **1** and **6** intramolecular hydrogens approach the nickel atoms (Table VII), further obstructing the coordination site about the plane of the inorganic core.

However, nickel exhibits low propensity for axial coordination relative to copper and zinc in related bis-diethyldithiocarbamate compounds (Ref. 72), which likely plays a large role in these heteroleptic analogues as well. The absence of stronger intermolecular interactions is responsible for the volatility of the nickel-containing compounds as discussed below.

Comparison of the two modifications of compound **2** reveals that the unit cell volume (1002.23 (18) Å^3) reported previously for **2b** (Ref. 60) is 4 percent larger than that (963.73(11) Å^3) for the structure **2a** determined here. A smaller cell is preferable as a larger volume allows for greater thermal motion and other disorder, and large temperature factors may afford bond distances smaller than the actual values (Ref. 73). Indeed, the isotropic temperature factors on the refined atoms of the published structure are about twice as large as those on corresponding atoms of structure **2a** with the smaller volume, and 10 of the 11 unique bond distances between refined positions reported for modification **2b** are smaller than those determined for **2a**. More efficient packing in the smaller cell also would allow greater intermolecular interactions, decreasing volatility as discussed below. Otherwise, the structures of the two modifications are similar, with the most significant difference (over 4°) being the dihedral angle formed between the planes of the core structure and the aminoisopropyl group (Table VIII).

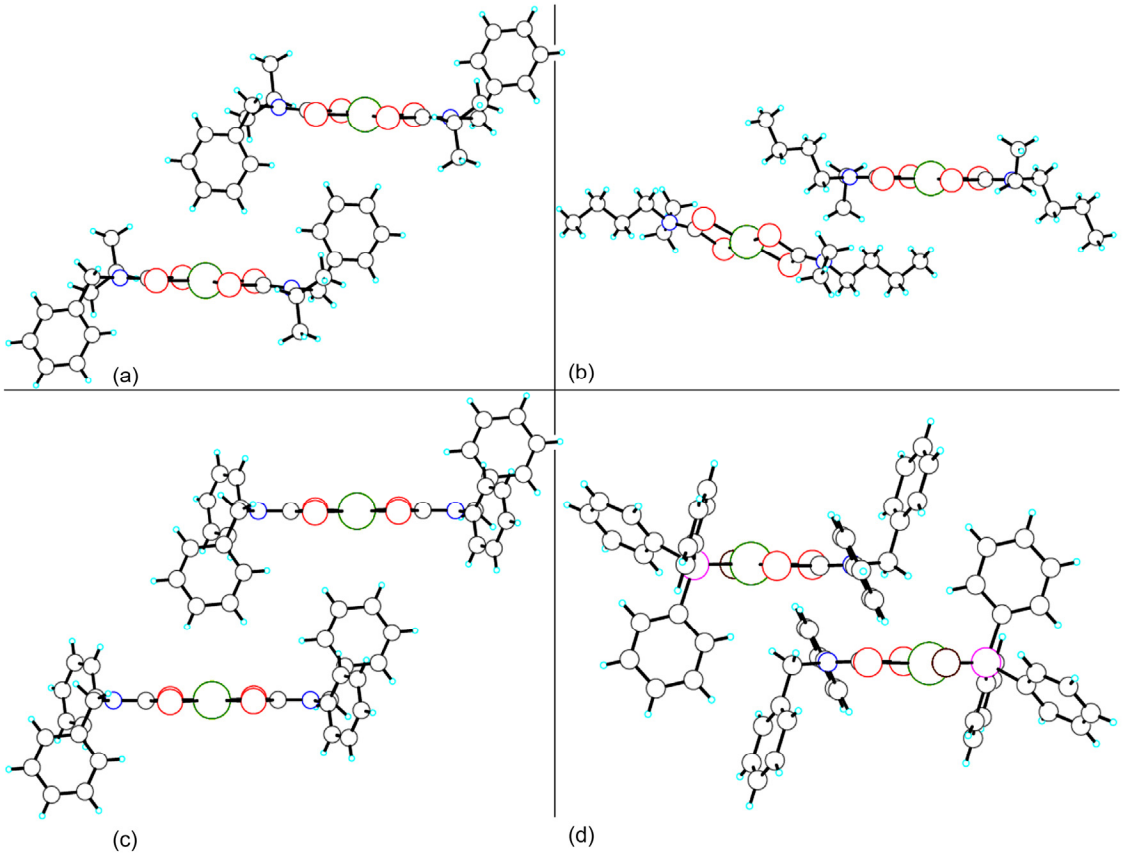

Figure 7.—Interaction diagrams showing close contacts to the core structures of synthesized dithiocarbamates. Nickel is represented by green circles; sulfur, by red; phosphorus, by magenta; carbon, by gray; nitrogen, by blue; and hydrogen, by cyan. (a) Ni(S_2CN(isopropyl)(benzyl))$_2$ **1**. (b) Ni(S_2CN(ethyl)(*n*-butyl))$_2$ **2a**. (c) Ni(S_2CN(phenyl)(benzyl))$_2$ **3**. (d) Ni(P(phenyl)$_3$)(S_2CN(phenyl)(benzyl))Cl **6**.

TABLE VIII.—DIHEDRAL ANGLES (°) BETWEEN SELECTED PLANES

Compound	Plane	Atoms in plane	Planes	Angle	Planes	Angle
1 Ni(dtc^{i}PrBz)$_2$	1	Ni,S11–S22,C10,C20	1,2	80.98(6)	2,4	135.90(16)
	2	C111–C116	1,3	109.05(5)	2,5	132.71(17)
	3	C211–C216	1,4	95.06(9)	3,4	17.92(9)
	4	C121–C123	1,5	96.59(9)	3,5	19.11(11)
	5	C221–C223	2,3	146.70(8)	4,5	3.7(2)
2 Ni(dtcEt^{n}Bu)$_2$	1	Ni,S1–S2,C1	1,2	85.81(15)[a]	---	87.08(16)[b]
	2	N1,C11–C14	1,3	92.99(18)[a]	---	97.1(2)[b]
	3	N1,C15–C16	2,3	64.42(13)[a]	---	65.42(16)[b]
3 Ni(dtcPhBz)$_2$	1	Ni,S1–S2,C1	1,2	82.08(5)	---	----------
	2	C11–C16	1,3	73.97(6)	---	----------
	3	C21–C26	2,3	64.14(7)	---	----------
6 Ni(dtcPhBz)(PPh$_3$)Cl	1	Ni,S1–2,P2,C1,C10	1,2	63.91(10)	2,6	43.05(12)
	2	C111–C116	1,3	108.31(9)	3,4	68.29(12)
	3	C121–C126	1,4	42.36(8)	3,5	102.34(12)
	4	C211–C216	1,5	84.96(7)	3,6	22.11(12)
	5	C221–C226	1,6	106.16(8)	4,5	106.35(10)
	6	C231–C236	2,3	46.61(13)	4,6	74.38(11)
	--	----------	2,4	34.43(12)	5,6	80.23(11)
	--	----------	2,5	84.89(11)	---	----------

[a]Compound **2a**, Ni(dtcEt^{n}Bu)$_2$.
[b]Corresponding positions for **2b**, with coordinates from Reference 60.

Thermal Analysis

TGA of metal dithiocarbamates, particularly bis(diorganodithio-carbamato)nickel(II) complexes, has been the topic of considerable research (Refs. 5, 15, 21, and 74 to 76). As stated in the introduction, research of numerous groups has focused on nickel(II) dithiocarbamates as precursors for various nickel sulfide phases (Refs. 14 to 17, 19, 21 to 23, and 77). TGA studies of nickel dithiocarbamates often yield complex results that are quite dependent upon molecular structural and experimental details (Ref. 75). In the intervening years after publication of a recent definitive review (Ref. 5), interest in decomposition of nickel dithiocarbamates and identification of nickel-containing products (Refs. 21 to 23, 50, 58, 64, and 77) has presented a variety of results and interpretations that encourage additional investigation. A summary of thermogravimetric results for the complexes **1** to **3**, **5**, and **6** studied is reported in Table IX; TGA plots are shown in Figure 8. Plots of the experimental results are reported in percentage of the original mass remaining, as is the first derivative of the percent mass remaining as a function of temperature; all derivative plots are to the same scale.

TABLE IX.—THERMOGRAVIMETRIC ANALYSIS (TGA) OF NICKEL DITHIOCARBAMATE COMPLEXES UNDER N_2

Compound (molecular weight)	Percent residue[a] (400 °C)	Percent residue[b,c] (temperature range, °C)	TGA derivative maximum,[c] °C	Theoretical residues,[d,e] percent
Ni(dtc^{i}PrBz)$_2$ **1** (507.43)	18.4	17.6 (260 to 440) 11.1 (440 to 1200)	343.3	20.0[f] **17.9**[g] 11.6[h]
Ni(dtcEt^{n}Bu)$_2$ **2a** (411.34)	21.2	13.7 (280 to 410) 8.7 (410 to 1200)	377.0	24.7[f] **19.5**[g] 14.3[h]
Ni(dtcPhBz)$_2$ **3** (575.46)	15.2	17.5 (260 to 430) 10.9 (430 to 1200)	341.1	17.6[f] **15.8**[g] 10.2[h]
Ni(dtcBz$_2$)$_2$ **5** (603.51)	13[i]	12.6 (215 to 420) 10 (420 to 975)	350.2	15.0[g] **13.3**[j] 9.7[h]
NiPPh$_3$(dtcPhBz)Cl **6** (614.82)	22.0	21.8 (215 to 475) 16.9 (475 to 1000) 12.9 (1000 to 1200)	296.1 323.2	**20.0**[k] 16.5[f] 13.0[j]

[a]Determined at NASA Glenn Research Center.
[b]Determined at Wheeling Jesuit University (WJU).
[c]Average of two measurements.
[d]Theoretical residue = (formula weight (FW) of NiS_x)/(molecular weight of compound).
[e]Bold indicates best fit considering experiments done both at WJU and NASA for homoleptic compounds (**1** to **3**, and **6**).
[f]Ni_3S_4; FW = 101.45 g/mol.
[g]NiS; FW = 90.77 g/mol.
[h]Ni; FW = 58.71 g/mol.
[i]Estimated from average of two runs at WJU.
[j]Ni_3S_2; FW = 80.08 g/mol.
[k]NiS_2; FW = 122.82 g/mol.

Figure 8(a) shows a TGA plot for Ni(dtc^{i}PrBz)$_2$ **1**. There are two well-defined mass losses at 204 and 343 °C. The small mass loss at 204 °C (2.1 percent) is unexplained, but not unprecedented (Refs. 5 and 63). It is followed by a large mass loss in the range of 260 to 440 °C (max. 343 °C) resulting in a residue at 437 °C of 17.6±0.5 percent, which corresponds closely to that calculated for NiS (17.9 percent). A gradual mass loss with increasing temperature continues, reaching a residue of 11.1±0.6 percent at 1200 °C, close to that calculated for Ni (11.6 percent). This result is in agreement with a simpler experiment at NASA GRC that resulted in a residue of 18.4 percent at 400 °C, within error for calculated mass of NiS and consistent with independent XRD analysis in a pyrolysis experiment; see below. Compound **1** had been included in an earlier study by Kameníček and Duffy (Ref. 63). The reported thermal decomposition of the complex begins at 80 °C and exhibits a plateau in the interval 410 to 460 °C (mass loss 73.7 percent; NiS_2: calculated 73.8 percent; $Ni(SCN)_2$: calculated 63.5 percent); decomposition was not complete until 1000 °C (Ref. 63). These results are not directly comparable since this experiment was carried out in air; also, there was no independent identification of the phases produced. The similar Ni(dtc^{n}BuBz)$_2$ was reported recently along with its TGA (Ref. 64). Decomposition starts at 237 °C and is

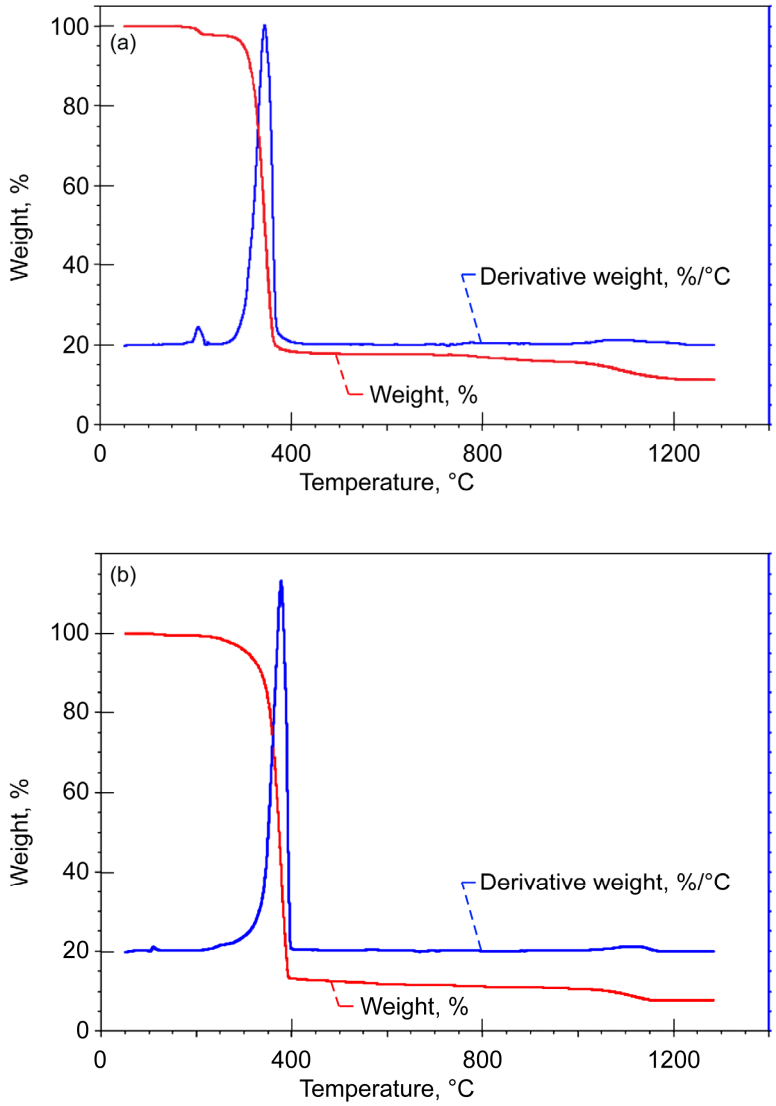

Figure 8.—Thermogravimetric analyses (with first derivatives) for synthesized dithiocarbamates. (a) Ni(S_2CN(isopropyl)(benzyl))$_2$ **1**. (b) Ni(S_2CN(ethyl)(*n*-butyl))$_2$ **2a**.

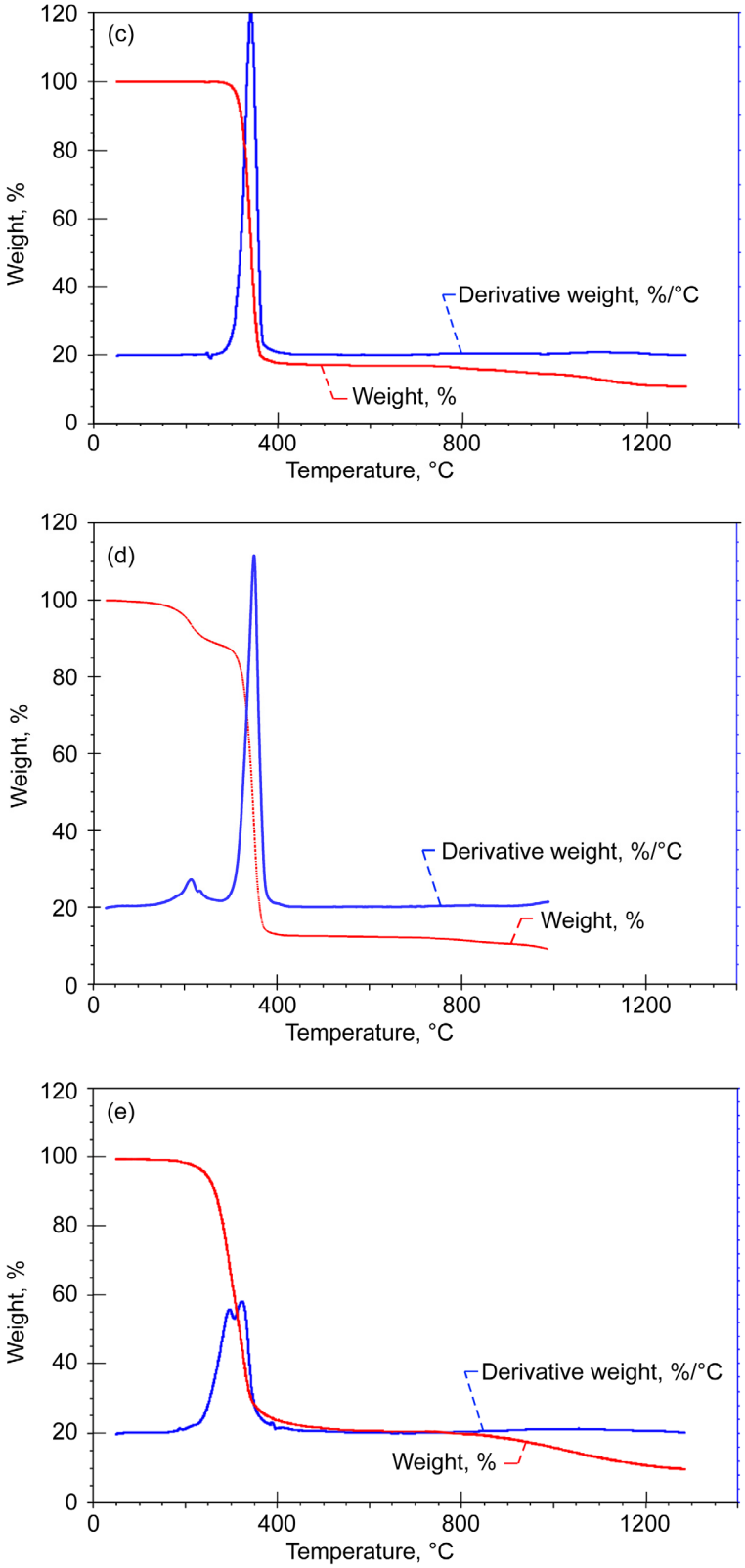

Figure 8.—Concluded. Thermogravimetric analyses (with first derivatives) for synthesized dithiocarbamates.
(c) $Ni(S_2CN(phenyl)(benzyl))_2$ **3**. (d) $Ni(S_2CN(benzyl)_2)_2$ **5**.
(e) $Ni(P(phenyl)_3)(S_2CN(phenyl)(benzyl))Cl$ **6**.

accompanied by three small exotherms. The exotherm at 508 °C was also found to be consistent with proposed formation of NiS_2 (or possibly $Ni(SCN)_2$), followed by oxidation to likely produce NiO which is thermally stable to 1050 °C. Again, these results were not carried out under inert atmosphere and were not independently verified by XRD on the pyrolysate or other method(s). In both of these earlier studies, it is likely that initial production of sulfides (or thiocyanates) is followed by oxidation; see results and discussion below.

It is instructive to consider the work of Cavalheiro and co-workers on the TGA and DSC of $Ni(S_2CN(CH_2)_4)_2$ and $Ni(S_2CN(CH_2)_5)_2$ in air and in N_2; results were quite different for the two ambient gases (Ref. 78). Thermolysis under N_2 of $Ni(S_2CN(CH_2)_4)_2$ produced results consistent with the proposed path: $Ni(S_2CN(CH_2)_4)_2 \rightarrow Ni(SCN)_2$ (284 to 374 °C) $\rightarrow$ NiS (374 to 405 °C) $\rightarrow$ Ni (405 to 690 °C), while the end product was primarily NiO in air. For $Ni(S_2CN(CH_2)_5)_2$, the proposed path was $Ni(S_2CN(CH_2)_5)_2 \cdot H_2O \rightarrow Ni(pipdtc)_2$ (173 to 245 °C) $\rightarrow$ NiS (272 to 600 °C) $\rightarrow$ Ni + Ni_3S_2 (600 to 743 °C); in air, NiO was produced (Ref. 78).

Figure 8(b) shows a TGA plot for $Ni(dtcEt^nBu)_2$ **2**. It shows two unexplained (but reproducible) mass losses at 108 °C (0.55 percent) and 258 °C (1.7 percent), followed by a sharp mass loss in the range of 280 to 400 °C (max. 377 °C) reaching a residue of 13.7±0.7 percent, which corresponds closely to that calculated for Ni (14.3 percent). An unexplained mass loss continues to an 8.7 percent residue at 1200 °C. In contrast, results obtained at NASA (21.2 percent residue) are consistent with a mixture of phases: the thiospinel Ni_3S_4 (24.7 percent) and millerite NiS (19.5 percent). In fact, failure to rigorously exclude oxygen in one run resulted in production of NiO along with NiS, as discussed below.

The volatility of some nickel(II) dithiocarbamates has been reported for more than a century and has been discussed in literature reviews (Refs. 74 and 75). Riekkola and Makitie reported that the TGA of $Ni(dtc^iBu_2)_2$ exhibited a single peak at 390 °C with a mass loss of 93 percent (Ref. 79). In an earlier study which included the TGA of $Ni(dtc^nBu_2)_2$, Singhal et al. noted significant volatility of the complex, yielding a residue of 6.79 percent, in contrast to $Ni(dtcH^nBu)_2$ which yielded NiS, confirmed by XRD (Ref. 15).

Previously, O'Brien and coworkers reported that $Ni(dtcEt_2)_2$ and $Ni(dtcMeEt)_2$ underwent mass loss in the range of 300 to 375 °C leaving a 10 percent mass residue (Ref. 17); reduction to elemental Ni would have yielded a residue of 16.5 and 17.9 percent, respectively. Thermolysis of $Ni(dtcMe^nBu)_2$ and $Ni(dtcMe^nCy)_2$ resulted in mass loss in two stages, approximately 6.5 percent at around 200 °C and rapid mass loss once again from 300 to 375 °C leaving an approximate 10 percent residue; the expected residue of Ni would have yielded 15.3 and 13.4 percent mass remaining, respectively. For each compound, XRD analysis of thin films deposited by low-pressure chemical vapor deposition, exploiting the volatility of these compounds, identified the presence of hexagonal ($NiS_{1.03}$ or α-) NiS, sometimes combined with rhombohedral millerite (β-NiS) (Ref. 17); see discussion below.

Figure 8(c) shows that the TGA of $Ni(dtcPhBz)_2$ (**3)** exhibits a single, well-defined mass loss in the range of 260 to 430 °C (341 °C max.), losing 82.5±0.1 percent of its mass. The residue, 17.5 percent, is intermediate between the formula NiS (15.8 percent) and NiS_2 (21.3 percent) and quite close to that for Ni_3S_4 (17.6 percent). At 1200 °C, the residue is 10.9±0.3 percent, quite close to that calculated for Ni (10.2 percent). The mass loss for the related symmetrical compound **5** ($Ni(dtcBz_2)_2$) begins at 215 °C and results in a 11.5 percent mass loss by 280 °C, see Figure 8(d). A rapid onset of decomposition peaks at 350 °C, resulting in a net loss of ~87 percent mass. As seen in Table IX, this is greater mass loss than predicted for NiS, this was not observed in the unsymmetrical compounds (**1** to **3**). Both the more complex and greater than anticipated weight loss could be related to the symmetrical substitution. This is consistent with prior literature (Refs. 5, 17, 38, 74, 75, and 79).

Figure 8(e) shows TGA of NiCl(dtcPhBz)(PPh_3) **6**, which exhibits a small mass loss (1.5±0.4 percent) between 160 and 200 °C. Upon further heating, the complex loses additional mass in two well-defined temperature ranges of 217 to 306 °C (295 °C max.) and 306 to 475 °C (324 °C max.), yielding residues of 61.4±2.7 percent and 21.8±0.5 percent. It is difficult to interpret these results due to the similarity of the mass of chemical species that are potentially lost. For example, loss of PPh_3 or Cl–CSN(PhBz) results in a loss of ~262 daltons (43 percent); a residue of ~22 percent could be accommodated by a variety of Ni-containing materials.

Kameníček et al. reported the preparation and properties of the series NiX(dtc^{n}BuBz)PPh_3 (where X = Cl, Br, I and NCS) (Ref. 80). Thermolysis results indicate decomposition beginning at a slightly higher temperature range of 171 to 204 °C, apparently correlated with mass, with multiple exotherms in the range of 181 to 508 °C. Finally, thermolysis was reported of two structurally related heteroleptic series, NiX(dtcHPh)PPh_3 and NiX(dtcHBz)PPh_3 (where X = Cl, Br, I, and NCS) (Ref. 65). All began to decompose at lower temperatures (45 to 135 °C); again the processes were complicated with no obvious stable intermediates. This trend was noted by Singhal for nickel (di)butyl dithiocarbamates (Ref. 18) and Duffy et al. for tris-dithiocarbamates of In(III) and Ga(III) (Ref. 81): decomposition occurs at lower temperatures for complexes derived from primary versus secondary amines. Given the complicated decomposition of heteroleptic compounds, we did not pursue further studies of compound **6** and focused on the five homoleptic compounds as precursors to nickel sulfides.

As outlined in the experimental section, our preliminary TGA results are fairly consistent with formation of 1:1 NiS phases for complexes **1** to **3** and **5**, as mass residues are within ~7 percent of pyrolysate mass predicted for NiS. This can be contrasted with the heteroleptic complex (**6**) where a 33 percent differential is clearly inconsistent with production of a 1:1 phase. The relatively high conversions of these unsymmetrically substituted complexes, even **2a**, which is an isomer of bis(diisopropyldithiocarbamato)nickel(II), may result from their greater surface areas and packing efficiencies (Fig. 7). We discuss our more in-depth pyrolysis and solid-state materials studies of the thermolysis of five homoleptic nickel dithiocarbamates in the following section; a compilation of information regarding relevant nickel sulfide (and related) phases (Ref. 33) is included (Table X) to facilitate the follow-on discussions.

TABLE X.—SUMMARY OF INFORMATION ON VARIOUS NICKEL (SULFIDE) PHASES ADDRESSED IN THIS STUDY[a]

Common name(s)	Stoichiometry	Structural type	Crystalline symmetry space group name (number)	JCPDF/ICDD reference numbers	Maximum thermal stability, °C
Millerite β-NiS (LT)	NiS	NiS	Rhombohedral R3m (160)	12-0041 75-0612 86-2280	380
α-NiS (HT) $NiS_{1.03}$	NiS	NiAs	Hexagonal $P6_3/mmc$ (194)	02-1273 75-0613	800
Heazlewoodite	Ni_3S_2	Ni_3S_2	Rhombohedral R32 (155)	44-1418 73-0698	530
Godlevskite	Ni_9S_8	Ni_9S_8	Orthorhombic C222 (21)	22-1193 78-1886	400
Polydymite	Ni_3S_4	Fe_3O_4 (Spinel)	Cubic $Fd\bar{3}m$ (227)	43-1469 76-1813	360
Vaesite	NiS_2	FeS_2 (Pyrite)	Cubic $Pa\bar{3}$ (205)	11-0099	980
Nickel sulfate	$NiSO_4$	----------	Orthorhombic Cmcm (63)	13-0435	---------
Bunsenite	NiO	----------	Cubic $Fm\bar{3}m$ (225)	47-1049	---------

[a]See text discussions and references for more in-depth information. Maximum thermal stability comes from Reference 33.

Pyrolysis and Solids Analysis

Compounds **1** to **5** were packed into alumina (Al_2O_3) boats and heated in a tube furnace with flowing nitrogen or forming gas (4 percent H_2 in Ar) at a rate of 150 cm^3/min (or sccm) at 300 to 450 °C for 1 h. Table XI summarizes the experimental conditions, thermolysis results and materials (pyrolysate) characterization. Phase analysis was performed either through use of JADE XRD analysis software (Materials Data, Inc., Livermore, CA) or manually.

TABLE XI.—X-RAY (POWDER) ANALYSIS OF NICKEL DITHIOCARBAMATE PYROLYSATE PHASE AND CRYSTALLITE SIZES

Sample	Details	Manually indexed phase(s)[a]	Lattice type(s)[b]	JADE[c] or manual[a] quantitative phase analysis	Crystallite size and method used,[d,e] nm
Ni(^{i}PrBzdtc)$_2$ **1**	400 °C (N_2)	$NiS_{1.03}$	Hexagonal	$NiS_{1.03}$ (100%)[a]	36,[d] 200[e]
Ni(^{i}PrBzdtc)$_2$ **1**	400 °C (N_2)	$NiS_{1.03}$	Hexagonal	----------	53[e]
Ni(Et^{n}Budtc)$_2$ **2**	400 °C (N_2)	$NiS_{1.03}$	Hexagonal	$NiS_{1.03}$ (85%)[a]	33,[d] 125[e]
		NiO	Cubic	NiO (15%)[a]	18,[d] 125[e]
Ni(Et^{n}Budtc)$_2$ **2**	400 °C (N_2)	$NiS_{1.03}$	Hexagonal	α-NiS (84%)[a]	18[d]
		β-NiS	Rhombohedral	β-NiS (16%)[a]	33[d]
Ni(PhBzdtc)$_2$ **3**	400 °C (N_2)	β-NiS	Rhombohedral	β-NiS (55%)[a]	32,[d] 143[e]
		$NiS_{1.03}$	Hexagonal	$NiS_{1.03}$ (45%)[a]	37,[d] 143[e]
Ni(PhBzdtc)$_2$ **3**	400 °C (N_2)	β-NiS	Rhombohedral	----------	125[e]
		$NiS_{1.03}$	Hexagonal		
Ni(Et$_2$dtc)$_2$ **4**	350 °C (N_2)	α-NiS	Hexagonal	α-NiS (85%)[c]	28[d]
		β-NiS	Rhombohedral	β-NiS (15%)[c]	32[d]
Ni(Et$_2$dtc)$_2$ **4**	400 °C (N_2)	α-NiS	Hexagonal	α-NiS (95%)[c]	19[d]
		β-NiS	Rhombohedral	NiO (5%)[c]	19[d]
Ni(Et$_2$dtc)$_2$ **4**	450 °C (N_2)	α-NiS	Hexagonal	α-NiS (40%)[c]	24[d]
				NiO (43%)[c]	16[d]
				$NiSO_4$ (17%)[c]	13[d]
Ni(Et$_2$dtc)$_2$ **4**	300 °C (4% H_2/Ar)	β-NiS	Rhombohedral	β-NiS (>95%)[c]	30[d]
		Ni_9S_8	Orthorhombic	Ni_9S_8 (<5%)[c]	~34[d]
Ni(Et$_2$dtc)$_2$ **4**	325 °C (4% H_2/Ar)	Ni_9S_8	Orthorhombic	Ni_9S_8 (>98%)[c]	26[d]
		β-NiS	Rhombohedral	β-NiS (<2%)[a]	---------
Ni(Et$_2$dtc)$_2$ **4**	350 °C (4% H_2/Ar)	Ni_9S_8	Orthorhombic	Ni_9S_8 (>98%)[c]	31[d]
		Ni_3S_2	Rhombohedral	Ni_3S_2 (<2%)[a]	---------
Ni(Et$_2$dtc)$_2$ **4**	400 °C (4% H_2/Ar)	Ni_3S_2	Rhombohedral	Ni_3S_2 (100%)[c]	27[d]
Ni(Et$_2$dtc)$_2$ **4**	450 °C (4% H_2/Ar)	Ni_3S_2	Rhombohedral	Ni_3S_2 (100%)[c]	24[d]
Ni(Bz$_2$dtc)$_2$ **5**	325 °C (N_2)	β-NiS	Rhombohedral	β-NiS (79%)[c]	34[d]
		α-NiS	Hexagonal	α-NiS (21%)[c]	26[d]
Ni(Bz$_2$dtc)$_2$ **5**	350 °C (N_2)	α-NiS	Hexagonal	α-NiS (87%)[c]	21[d]
		β-NiS	Rhombohedral	β-NiS (13%)[c]	31[d]
Ni(Bz$_2$dtc)$_2$ **5**	400 °C (N_2)	α-NiS	Hexagonal	α-NiS (100%)[c]	24[d]

[a]Manually indexed using the following ICDD files: 02-1273 ($NiS_{1.03}$ ≈ α-NiS); 12-0041 (β-NiS or Millerite); 44-1418 (Ni_3S_2, Heazlewoodite); 47-1049 (NiO or Bunsenite); 78-1886 (Ni_9S_8 or Godlevskite).

[b]See discussion in text and Table X for crystal structural symmetry types.

[c]Phase determination and quantitative analysis using JADE software (Materials Data, Inc., Livermore, CA http://www.materialsdata.com/index.html) with the following (newer) ICDD files: 13-0435 (orthorhombic-$NiSO_4$); 47-1049 (NiO or Bunsenite). 73-0698 (Ni_3S_2, Heazlewoodite); 75-0613 (α-NiS); 78-1886 (Ni_9S_8 or Godlevskite); or 86-2280 (β-NiS or Millerite).

[d]Scherrer equation, see text.

[e]Brunauer, Emmett, and Teller (BET) analysis, see text.

Processing and Analysis Methods

The pyrolysis temperature was chosen based upon data from TGA experiments and the literature (Refs. 14 to 17) showing significant weight loss and essentially complete decomposition at temperatures below 400 °C (Table IX). Flowing nitrogen (forming gas) provides an inert (or a reducing) atmosphere and should preclude interaction with oxygen.

Scanning electron microscopy clearly demonstrates production of nanocrystals from microcrystalline dithiocarbamates; Figure 9 for compound **1** is typical of the morphology of precursors and pyrolysates. We attempted use of energy dispersive spectroscopy (EDAX Falcon model) to measure stoichiometry of pyrolysates. However, evolved gases were likely adsorbed onto the highly porous surface resulting in high concentrations of volatile elements (especially carbon and sulfur) relative to nickel.

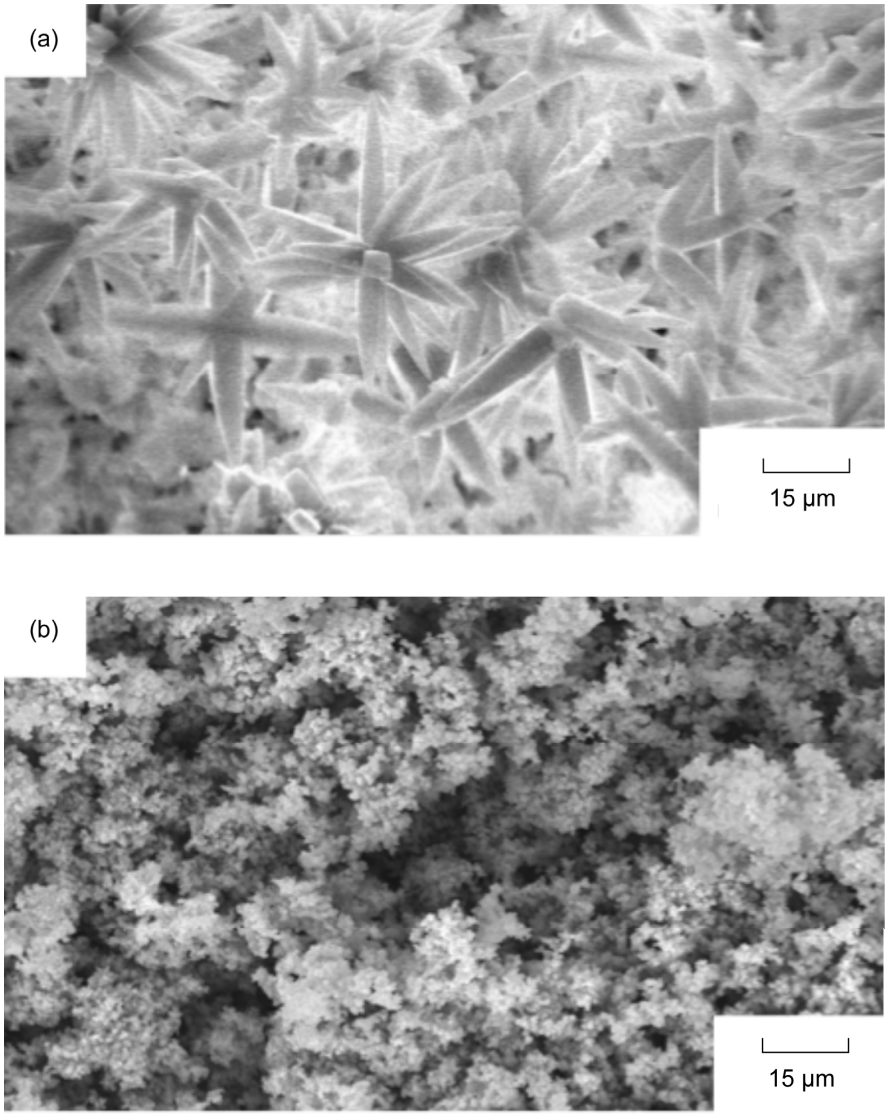

Figure 9.—Scanning electron micrographs before and after pyrolysis of $Ni(S_2CN(isopropyl)(benzyl))_2$ **1**, under conditions described in Tables IX and X. (a) Before. (b) After.

Powder XRD of pyrolysates produced during three different pyrolysis experiments allowed for identification of major phases of (nano)crystalline materials as shown in Figures 10 to 12. Decomposition products of three different unsymmetrically substituted dithiocarbamates (**1** to **3**) under flowing nitrogen at 400 °C was compared (Fig. 10). Products of the decomposition of both symmetrically substituted dithiocarbamates (**4** and **5**) under flowing nitrogen were compared at 325 to 450 °C (Fig. 11). Changes in decomposition products (nickel sulfide phases) of the diethyldithiocarbamate (**4**) under flowing forming gas (4 percent H_2 in Ar) are observed at 300 to 450 °C (Fig. 12).

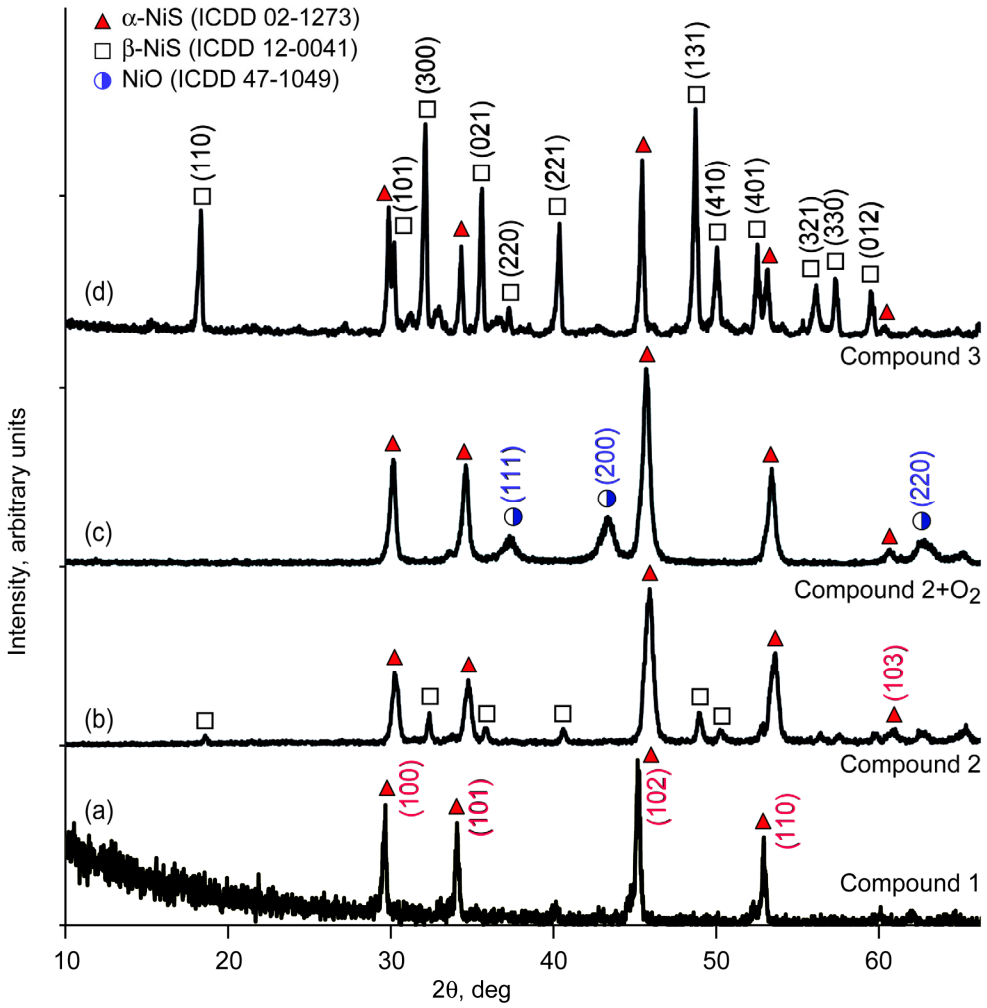

Figure 10.—X-ray powder diffractograms of pyrolysates of synthesized unsymmetric dithiocarbamates produced under nitrogen as described in Table XI. (a) $Ni(S_2CN(isopropyl)(benzyl))_2$ **1**. (b) $Ni(S_2CN(ethyl)(n\text{-}butyl))_2$ **2**, without oxygen. (c) Compound **2**, with oxygen. (d) $Ni(PhBzdtc)_2$ **3**.

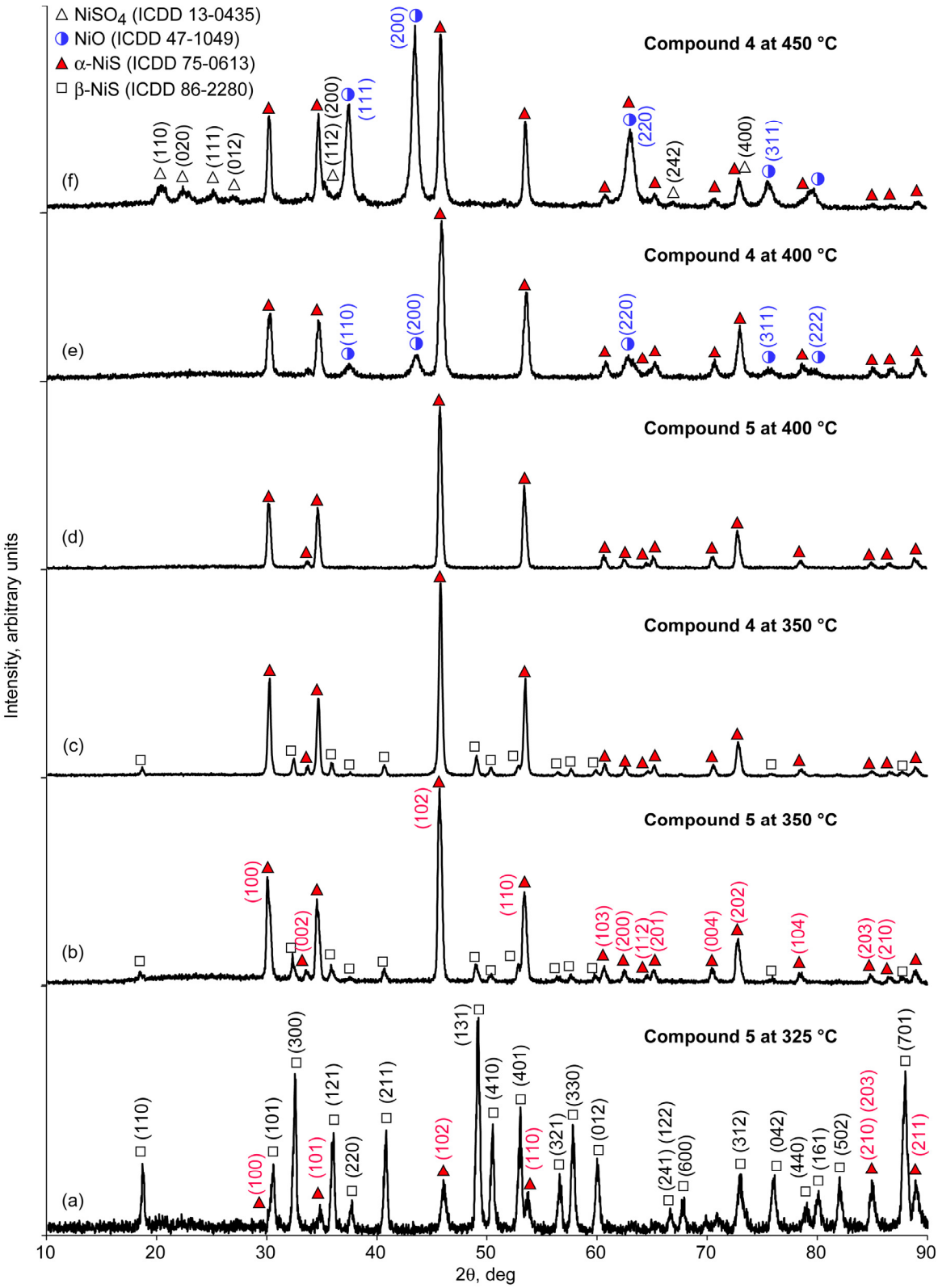

Figure 11.—X-ray powder diffractograms of the pyrolysates of synthesized symmetric dithiocarbamates produced under nitrogen as described in Table X. (a) $Ni(S_2CN(benzyl)_2)_2$ **5**, at 325 °C. (b) Compound **5**, at 350 °C. (c) $Ni(S_2CN(ethyl)_2)_2$ **4**, at 350 °C. (d) Compound **5**, at 400 °C. (e) Compound **4**, at 400 °C. (f) Compound **4**, at 450 °C.

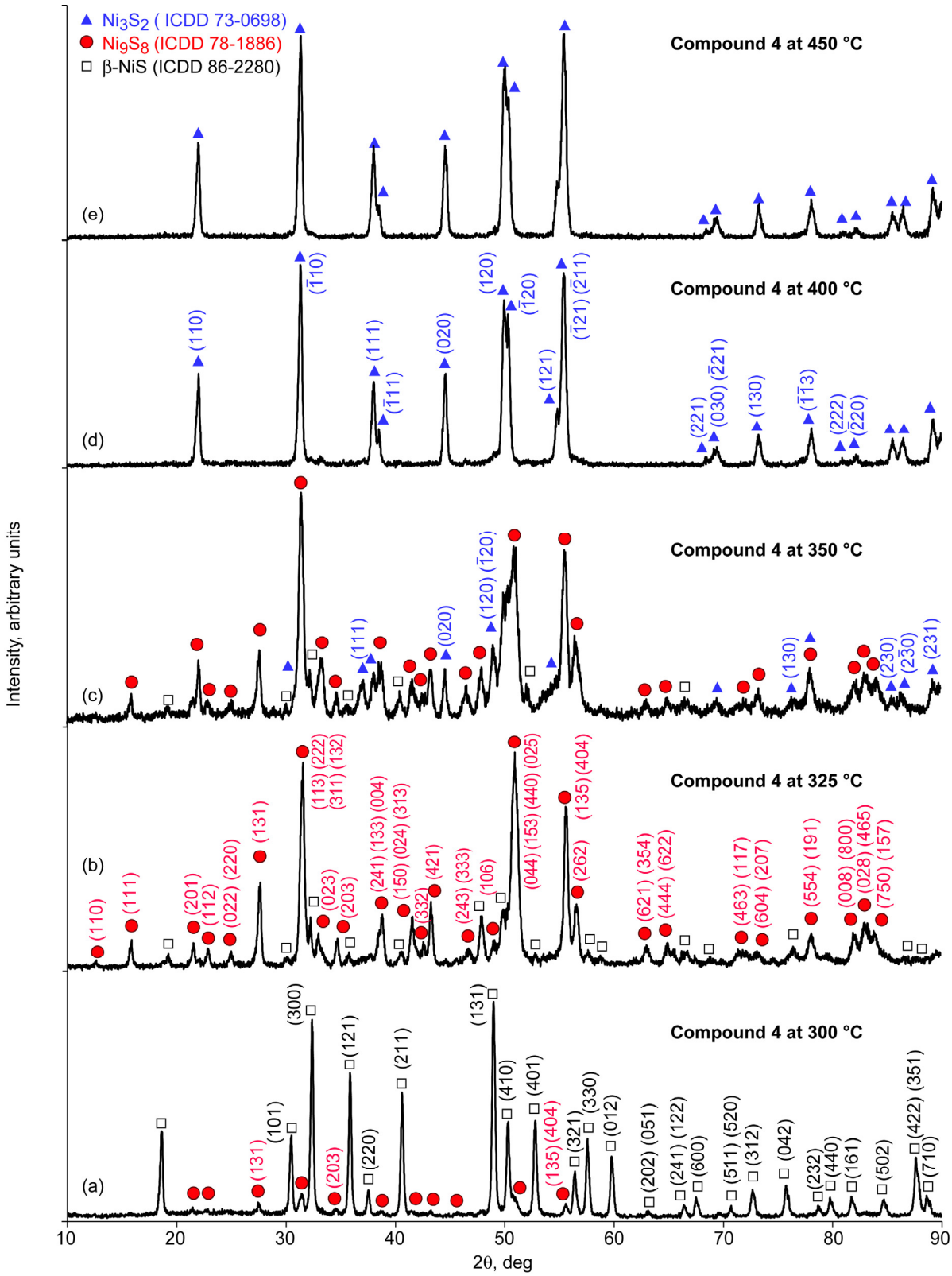

Figure 12.—X-ray powder diffractograms of the pyrolysate of $Ni(S_2CN(ethyl)_2)_2$ **4**, under flowing forming gas (4 percent hydrogen in argon) as described in Table XI. (a) 300 °C, (b) 325 °C, (c) 350 °C, (d) 400 °C, and (e) 450 °C.

Phase Analyses

Manual phase identity was accomplished by comparison to JCPDF or ICDD card data. A reference-intensity-ratio method of semiquantitative XRD analysis was used to estimate the composition of the multiphase samples based upon relative intensities of the most intense peaks compared to intensities published in the ICDD standards (Ref. 82). This method should be considered as only semiquantitative (Ref. 83).

In the first experiment (Fig. 10), two separate thermolyses were done for dithiocarbamate complex **1** to **3** to ensure that temperature variations were averaged out, sufficient pyrolysate was produced to analyze, and to guard against potential oxygen contamination. In fact, trial one of compound **2** resulted in a failure to completely exclude oxygen and production of cubic NiO (ICDD 47-1049). A comparison of weight loss in Tables IX and XI shows good agreement for compounds **1** and **3** but that excess weight remained for decomposition of compound **2** after 1 h; production of NiO likely accounts for poor agreement between pyrolysis and TGA experiments.

The low-temperature (rhombohedral) phase of (β-)nickel sulfide (millerite) converts to the hexagonal or α-NiS ($NiS_{1.03}$) phase at 379 °C (Ref. 31). In our thermolysis experiments, the hexagonal phase predominated, although there was significant millerite found when compound **3** was used as a precursor. While there was no correlation of product mix with maximum weight loss in TGA, there may be some impact of the precursor molecular weight; the all-aromatic compound **3** produced an approximate 50/50 mix of millerite and α-NiS (see further discussion below). However, there is enough error in the temperature sensor and variation in the thermolysis conditions to equivocate on this conclusion. The adventitious oxidation in trial one of compound **2** resulted in conversion of only the rhombohedral or lower temperature stable-millerite to NiO.

The second experiment (Fig. 11), also under nitrogen, examined decomposition of the symmetrically substituted compounds (**4** and **5**) as a function of temperature. Rhombohedral millerite (β-NiS) was the dominant phase only at 325 °C for decomposition of **5**. By 350 °C, decomposition of both diethyl (**4**) and dibenzyl (**5**) compounds produced the hexagonal phase at ~85 percent abundance. At 400 °C, both compounds produced the hexagonal phase exclusively. Deomposition at a higher temperature (450 °C) under an oxygen-containing atmosphere produced the hexagonal phase, NiO (as observed for **2** above), and also $NiSO_4$, see Table XI.

Finally, decomposition of **4** under forming gas from 300 to 450 °C produced almost single-phase millerite (300 °C), nearly pure orthorhombic godlevskite (Ni_9S_8) at 325 and 350 °C, and single-phase rhombohedral heazlewoodite (Ni_3S_2) at temperatures of 400 and 450 °C. The presence of hydrogen in the atmosphere facilitates loss of sulfur (presumably as H_2S), producing nickel-rich phases, see Figure 12 and Table XI.

Crystallite and Particle Size Analyses

An estimate of the minimum crystallite size (diameter, *D*) was determined by use of the Scherrer formula (Eq. (1)). The constant (*K*) is a shape factor and typically ranges from 0.87 to 1 (we used the average value (0.94)); λ is the X-ray wavelength (Cu K_α = 1.5418 Å); β is the full-width half-maximum of a peak in radians; and θ is the Bragg angle of the peak (Ref. 84).

$$D_S = K \cdot \lambda / \beta \cdot \cos\theta \tag{1}$$

Each estimated minimum crystallite size is the mean of 3 to 5 of the most intense unambiguous peaks for each phase. Scherrer's formula often underestimates crystallite size; there can be a significant contribution to β from instrumental effects (Ref. 76). Thus, our results should be viewed as representing minimum size.

An alternative method utilizing the surface area (*SA*) measured by the Brunauer, Emmett, and Teller (BET) gaseous method employs Equation (2) (Ref. 85), commonly expressed as

$$D_{BET} = 6000/\rho \cdot SA \tag{2}$$

ρ is the theoretical density (for nickel sulfides, ρ = 6 g/cm^3), and *SA* is in units of g/cm^2. The number produced by this equation is in units of nm; see Table XI. Finally, transmission electron microscopy (TEM) can be utilized to directly examine the particle sizes and distributions, see Figures 13 and 14, respectively, for typical results.

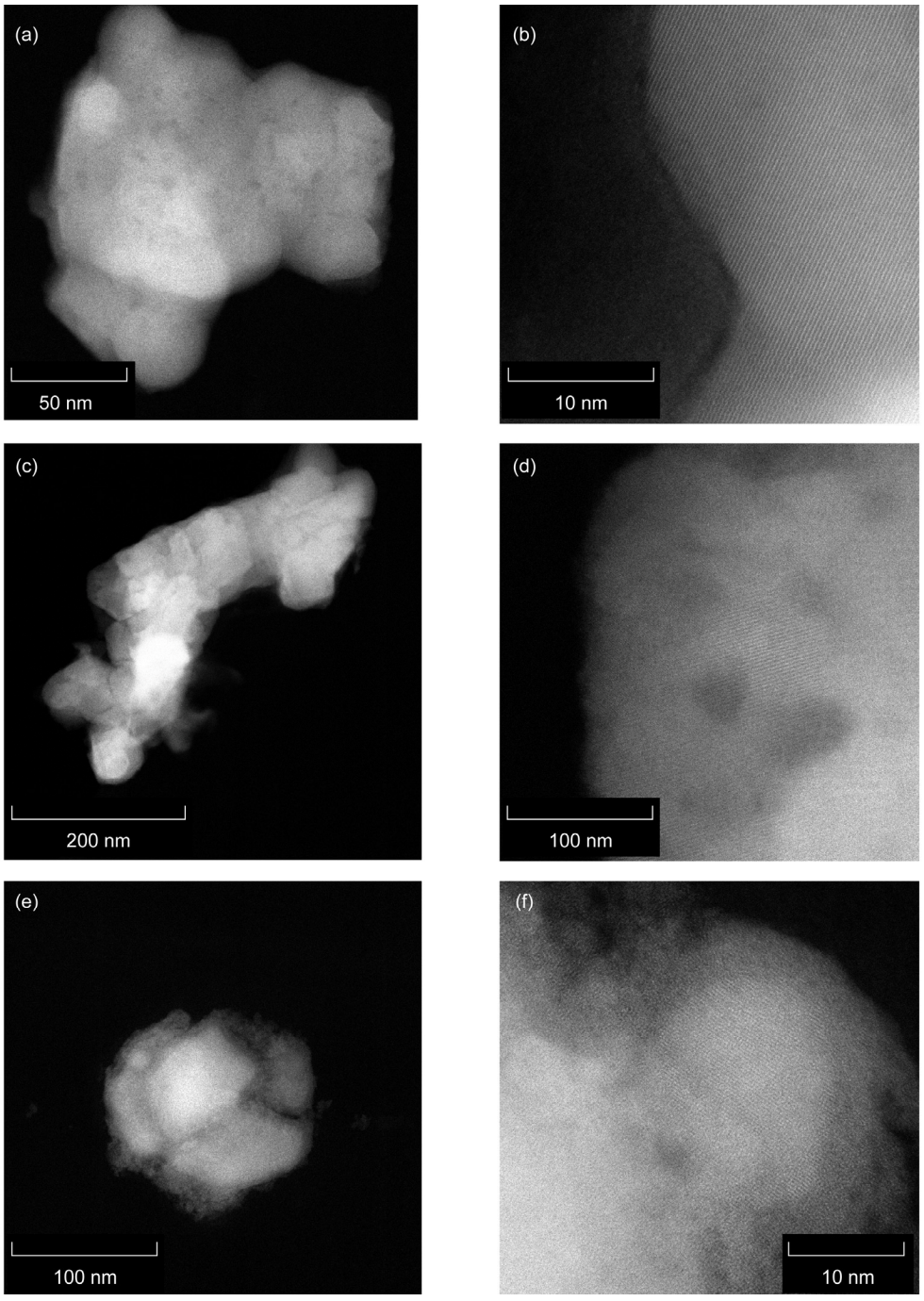

Figure 13.—Transmission electron micrographs of synthesized dithiocarbamate samples after pyrolysis for 1 h under nitrogen showing clumps of smaller crystallites combining to form larger agglomerates and, under higher magnification, planes of individual crystallites. (a) Ni(S_2CN(ethyl)(*n*-butyl))$_2$ **2**, at 400 °C. (b) Compound **2** (400 °C) at higher magnification. (c) Ni(S_2CN(ethyl)$_2$)$_2$ **4**, at 400 °C. (d) Compound **4** (400 °C) at higher magnification. (e) Compound **4,** at 450 °C. (f) Compound **4** (450 °C) at higher magnification.

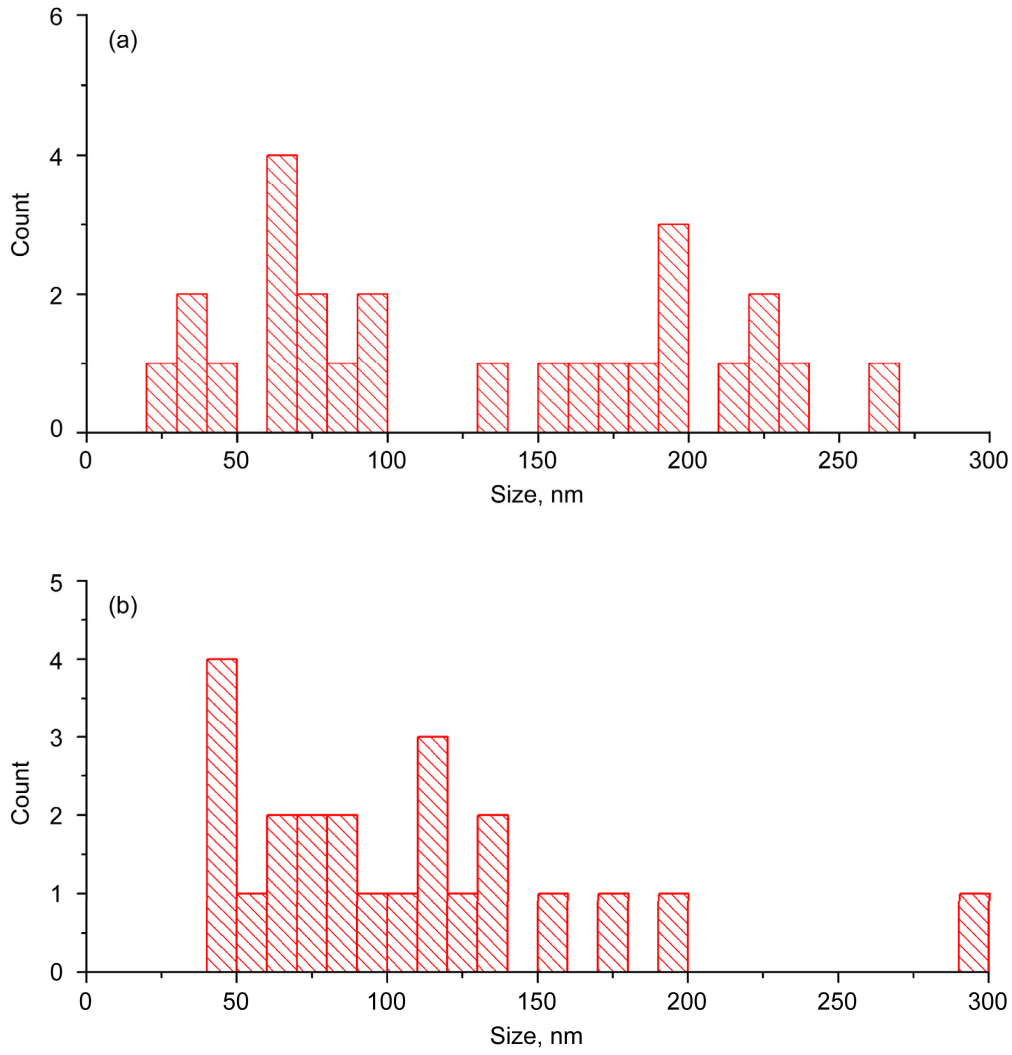

Figure 14.—Representative particle size distribution observed in transmission electron micrographs (see Fig. 13). (a) $Ni(S_2CN(ethyl)(n\text{-butyl}))_2$ **2**, pyrolized at 400 °C for 1 h under nitrogen. (b) $Ni(S_2CN(ethyl)_2)_2$ **4**, pyrolized at 400 °C for 1 h under nitrogen.

Clearly, as seen in Figure 13, the larger particles are aggregates of crystallites that seem to range in size from ~20 to 50 nm. Given the nature of the samples being examined, it is more likely that BET surface area measurements are describing particles or crystallite agglomerates. We can estimate that a 125 nm particle can contain up to 200 crystallites of an average size of 30 nm. It is clear from the TEM results that there is a range of sizes or distribution produced for not only the particles (agglomerates) but also the crystallites. A more in-depth treatment and analysis of particle sizes is beyond the scope of this study.

Discussion

Table XII is a compilation of results from our work and earlier studies (Refs. 14 to 17, 19, and 21 to 23). Wold et al. decomposed nickel bis(diethyldithiocarbamate) under flowing H_2S at 200 °C and completed the experiment at 500 °C producing Ni_3S_2 (Ref. 14). We had the same result using the same compound (**4**) under forming gas. Singhal et al. decomposed homoleptic bis-butyl- and bis-dibutyl-nickel dithiocarbamates by TGA (under 7 percent H_2/N_2 or N_2) and heated stage-XRD under 7 percent H_2/N_2 up to 500 °C to produce millerite (rhombohedral or β-NiS – ICDD 12-0041) and a poorly characterized

TABLE XII.—COMPARISON OF PYROLYSIS, DECOMPOSITION, OR DEPOSITION RESULTS OF NICKEL SULFIDES FROM DITHIOCARBAMATE PRECURSORS FROM THE LITERATURE AND THIS WORK

Precursor compound	Decomposition conditions[a,b]	Temperature,[c] °C	Phase(s) produced[d]	Appearance or morphology[c]	Text reference
$Ni(Et_2dtc)_2$	Pyrolysis at 200 °C under H_2S, then at 525 °C under H_2/H_2S (125:1)	200; 525	Ni_3S_2	----------	14
$Ni(^nBu(H)dtc)_2$	Heated stage XRD (7% H_2/N_2)	100 to 200	NiS*	----------	15
$Ni(^nBu(H)dtc)_2$	Heated stage XRD (7% H_2/N_2)	250 to 300	β-NiS	----------	15
$Ni(^nBu(H)dtc)_2$	Heated stage XRD (7% H_2/N_2)	350 to 450	$Ni_3S_2 + Ni_7S_6$	----------	15
$Ni(^nBu(H)dtc)_2$	Heated stage XRD N_2	350	NiS* + β-NiS	----------	15
$Ni(Et_2dtc)_2$ **4**	Pyrolysis under 150 sccm (4% H_2/Ar)	300	β-NiS	Clumps of nanoparticles	**This work**
$Ni(Et_2dtc)_2$ **4**	Pyrolysis under 150 sccm (4% H_2/Ar)	325 and 350	Ni_9S_8	Clumps of nanoparticles	**This work**
$Ni(Et_2dtc)_2$ **4**	Pyrolysis under 150 sccm (4% H_2/Ar)	400 and 450	Ni_3S_2	Clumps of nanoparticles	**This work**
$Ni(Et_2dtc)_2$	CVD: 120 Pa N_2 on Si(111)	Source: 250 Substrate: 350 to 400	$NiS_{1.03}$	Needles and leafs	16
$Ni(Et_2dtc)_2$	CVD: 1.5 Pa N_2 on glass	Source: 200 to 250 Substrate: 400 to 450	$NiS_{1.03}$ + β-NiS (minor)	Needles, nanowires and platelets	17
$Ni(MeEtdtc)_2$	CVD: 1.5 Pa N_2 on glass	Source: 250 Substrate: 450	$NiS_{1.03}$	Needles and platelet clumps	17
$Ni(Me^nBudtc)_2$	CVD: 1.5 Pa N_2 on glass	Source: 275 Substrate: 450	$NiS_{1.03}$	Nanowires and clumps	17
$Ni(Et_2dtc)_2$ $Ni(MeEtdtc)_2$ $Ni(Me^nHexdtc)_2$	Spray: 140 sccm Ar on glass	Source: 25 Substrate: 400	$NiS_2 + Ni_7S_6$	Tangles of wires	19
$Ni(Et_2dtc)_2$ $Ni(MeEtdtc)_2$ $Ni(Me^nHexdtc)_2$	Spray: 140 sccm Ar on glass	Source: 25 Substrate: 425	$NiS_{1.03}$ (major) + NiS_2 + Ni_7S_6	Tangles of wires	19
$Ni(Et_2dtc)_2$ $Ni(MeEtdtc)_2$ $Ni(Me^nHexdtc)_2$	Spray: 140 sccm Ar on glass	Source: 25 Substrate: 450	$NiS_{1.03}$	Tangles of wires	19
$Ni(Me^nBudtc)_2$	Spray: 140 sccm Ar on glass	Source: 25 Substrate: 400 to 425	$NiS_2 + Ni_7S_6$	Tangles of wires	19
$Ni(Me^nBudtc)_2$	Spray: 140 sccm Ar on glass	Source: 25 Substrate: 450	(200)-NiS_2	Hexagonal grains and wires	19
$Ni(Bz_2dtc)_2$ **5**	Pyrolysis under 150 sccm N_2	325	β-NiS (major) + $NiS_{1.03}$	Clumps of nanoparticles	**This work**
$Ni(Et_2dtc)_2$ **4** $Ni(Bz_2dtc)_2$ **5**	Pyrolysis under 150 sccm N_2	350	$NiS_{1.03}$ (major) + β-NiS	Clumps of nanoparticles	**This work**
$Ni(Bz^iPrdtc)_2$ **1**, **4**, and **5**	Pyrolysis under 150 sccm N_2	400	$NiS_{1.03}$	Clumps of nanoparticles	**This work**

TABLE XII.—Concluded.

Precursor compound	Decomposition conditions[a,b]	Temperature,[c] °C	Phase(s) produced[d]	Appearance or morphology[c]	Text reference
Ni(^{n}BuEtdtc)$_2$ **2**	Pyrolysis under 150 sccm N_2	400	$NiS_{1.03}$ (major) + β-NiS	Clumps of nanoparticles	**This work**
Ni(BzPhdtc)$_2$ **3**	Pyrolysis under 150 sccm N_2	400	β-NiS (major) + $NiS_{1.03}$	Clumps of nanoparticles	**This work**
Ni(^{i}Bu$_2$dtc)$_2$	Solvothermal pyrolysis (N_2) in n-hexylamine	120	α-NiS (major) + Ni_3S_4	Clumps of nanospheres	21
Ni(^{i}Bu$_2$dtc)$_2$	Solvothermal pyrolysis (N_2) in oleylamine	150	α-NiS	Clumps of nanospheres	21
Ni(^{n}Hex(H)dtc)$_2$	Solvothermal pyrolysis (N_2) in dodecane	120	Ni_3S_4	Clumps of nanospheres	21
Ni(Bz^{n}Budtc)$_2$	Solvothermal pyrolysis (N_2) in EtOH/$CHCl_3$ (5:1)	160	NiS_2 (major) + β-NiS	Clumps of nanospheres	22
Ni($CS_2NC_4NC(H)Ph_2$)$_2$	Solvothermal pyrolysis (N_2) in EtOH/$CHCl_3$ (5:1)	400	NiS_2:Ni_3S_4 (70:30)	Clumps of nanospheres	23

[a]Atmosphere for decomposition is under either inert (N_2 or Ar) or reducing (4% H_2/Ar, 7% H_2/N_2, or H_2/H_2S) conditions.
[b]XRD is X-ray diffraction and CVD is chemical vapor deposition.
[c]See individual references for more detailed experimental descriptions.
[d]NiS* is a poorly defined phase, other phases are further described in text references.

related phase (ICDD 02-1280) and several nickel-rich phases (Ni_3S_2 and Ni_7S_6) through loss of H_2S (Ref. 15). Nomura and Hyata studied the deposition of hexagonal phase (α-NiS or $NiS_{1.03}$ – ICDD 02-1273) films using the same compound Ni($S_2CN(C_2H_5)_2$)$_2$ on Si(111) substrates at 350 to 400 °C by low pressure chemical vapor deposition (CVD) (Ref. 16).

O'Brien and coworkers reported synthesis and characterization of homoleptic symmetrically and unsymetrically substituted nickel(II) dithiocarbamates (Ref. 19) and use of nickel dithiocarbamates as precursors for several different nickel sulfides ($NiS_{1.03}$, β-NiS, NiS_2, and α-Ni_7S_6) (Refs. 17 and 19). Using a CVD process at a lower pressure of carrier gas (1.5 Pa N_2) resulted primarily in the production of the hexagonal α-NiS or $NiS_{1.03}$ phase (Ref. 17). This agrees with our own results using both symmetrically and unsymmetrically substituted nickel dithiocarbamates and Nomura (Ref. 16). Spray pyrolysis of three different alkyl nickel dithiocarbamates (RR′ = Et_2, MeEt, or Me^{n}Hex) on glass substrates using an Ar carrier gas produced a mixture of Ni_7S_6 and NiS_2 at 400 °C, mostly $NiS_{1.03}$, Ni_7S_6 and NiS_2 at 425 °C and hexagonal $NiS_{1.03}$ at 450 °C (Ref. 19). Using Ni(dtcMe^{n}Bu)$_2$ as a precursor produced a mixture of Ni_7S_6 and NiS_2 at 400 and 425 °C; NiS_2 was produced at 450 °C (Ref. 19).

Recently, two groups have utilized nickel dithiocarbamates as single-source precursors under inert atmospheres under solvothermal reaction conditions. Hogarth et al. published a very interesting, in-depth and well-designed mechanistic study of the decomposition of nickel dithiocarbamates under a variety of solvothermal reaction conditions (Ref. 21). When symmetrically substituted Ni(dtc^{i}Bu$_2$)$_2$ was heated in liquid amine at 120 °C, mainly hexagonal α-NiS and some Ni_3S_4 were produced; at 150 °C, the product was hexagonal α-NiS (Ref. 21). Unsymetrically substituted Ni(dtc^{n}Hex(H))$_2$ heated in dodecane at 120 °C produced Ni_3S_4 (Ref. 21). Prakasam and colleagues from Finland studied the decomposition of an unsymmetrically substituted complex related to compound **1** (Ni(dtc^{n}BuBz)$_2$) at 160 °C in EtOH/$CHCl_3$ (5:1) and noted the production of nanoclumps of primarily vaesite (NiS_2) with a minority fraction of millerite (β-NiS) (Ref. 22). The same group conducted a related study in the same mixed solvent using Ni($CS_2NC_4NC(H)Ph_2$)$_2$, a 4-(diphenyl-methyl)piperazinecarbodithioato complex, at 400 °C and produced a 70/30 mixture of NiS_2 and Ni_3S_4 (Ref. 23).

Every precursor compound decomposed in this study or reported in the literature begins with a core NiS_4 stoichiometry. However, as discussed above, the initial decomposition pathways may be influenced by precursor structure. As demonstrated quite convincingly by the Exxon Research group (Ref. 15) for simple thermolysis, Hogarth (Ref. 21) for solvothermal decomposition, and O'Brien (Ref. 86) for thin film deposition by CVD or spray pyrolysis, reaction conditions are much more important for determining sulfide phase(s) produced.

The main insight derived from analyzing phase production under a variety of conditions from this work and previous studies (Refs. 14 to 17, 19, and 21 to 23) is that three general growth or deposition patterns emerge. For powder thermolysis or CVD from a heated source under nitrogen, the products are determined primarily by thermodynamic considerations (this work and Refs. 15 to 17) of the sulfide product regardless of precursor structure, unsymmetrical, symmetrical, mono- or bis-dithiocarbamate (Table XI). Flowing inert gas transports sulfur-containing byproducts and 1:1 molar ratio phases (α-NiS and β-NiS) are produced; as expected the hexagonal phase predominates at temperatures over 380 °C (Ref. 33), see Table X. Use of forming gas (or H_2S) produces nickel-rich sulfide phases through enhanced loss of sulfur, presumably as H_2S (this work and Refs. 14 and 15). Initially formed millerite (β-NiS) decomposes to form godlevskite (Ni_9S_8); this slightly nickel-rich phase further reacts and produces heazlewoodite (Ni_3S_2), a phase stable at temperatures up to 530 °C (Ref. 33).

Spray pyrolysis (starting with an unheated precursor) (Ref. 19) or solvothermal reactions (Refs. 21 to 23) produce a complex mixture of nickel sulfides. Loss of sulfur occurs as solid-state phases are produced during film deposition; vaesite (NiS_2) is the most often formed phase at 400 or 425 °C; the hexagonal (α-)NiS phase is most prevalent at 450 °C. This can be rationalized by the stability of these two phases (Ref. 33) and the enhanced loss of sulfur expected at the higher deposition temperature (Ref. 86).

For solvothermal studies, sulfur partial pressures are expected to be higher, and the solvent or reaction medium will definitely play an important role in determining the nickel sulfide phases produced (Refs. 21 to 23). Decomposing $Ni(dtc^{n}Hex(H))_2$, a monosubstituted dithiocarbamate, in dodecane at 120 °C produces the thiospinel phase (Ni_3S_4). Use of a primary amine as the reaction medium resulted in decomposition of the symmetrically disubstituted $Ni(dtc^{i}Bu_2)_2$ to yield a mixed-phase (α-NiS (major) and Ni_3S_4) product at 120 °C that became pure α-NiS at 150 °C (Ref. 21). This is consistent with the greater known stability of the hexagonal 1:1 phase (Ref. 33).

Finally, two recent reports on decomposition of two different structural types of nickel dithiocarbamates in $EtOH/CHCl_3$ (5:1) produced NiS_2 as the major product with β-NiS and Ni_3S_4 as minor products at 160 °C (Ref. 22) and 400 °C (Ref. 23), respectively. The main observation to be made from the two studies from Finland is that vaesite is the predominant (and most stable (Ref. 33)) sulfur-rich product. Clearly, the use of solvothermal reaction conditions warrants further study as this approach offers opportunities for enhanced control of phase and morphology.

Conclusions

A slightly distorted square-planar nickel coordination environment is observed for all four unsymmetrically substituted nickel(II) dithiocarbamate complexes studied: $Ni(S_2CN(isopropyl)(benzyl))_2$ **1**, $Ni(S_2CN(ethyl)(n\text{-butyl}))_2$ **2**, $Ni(S_2CN(phenyl)(benzyl))_2$ **3**, and $Ni(P(phenyl)_3)(S_2CN(phenyl)(benzyl))Cl$ **6**. Compound **1** exhibits the greatest asymmetry of the Ni–S bonds amongst the homoleptic compounds, and a trans-influence affects the Ni-S bond distances in compound **6**.

Electronic absorption spectra include a weak d-d band(s), one strong metal-ligand charge transfer band, and three intense intra-ligand charge transfer bands, as observed previously. Solid-state infrared spectra in both the C–S and C–N regions are more complex because of the lower symmetry and presence (for complexes **1**, **3**, and **6**) of aromatic spectral features but are essentially consistent with previous reports.

The organic residues adopt conformations (transoid and anti) to minimize steric interactions. Steric effects also may determine the puckering of the nickel and nitrogen atoms, both being planar or nearly so. The nitrogens essentially form double bonds to the CS_2 carbons. The other substituents on nitrogen in **1** to **3** adopt transoid conformations. There are no strong intermolecular interactions, consistent with previous reports of the volatility of these compounds.

Thermogravimetric analyses are consistent with production of 1:1 NiS phases under inert atmospheres or nickel-rich phases under reducing conditions, pointing to the utility of these complexes for the fabrication of solid-state materials. The priority of processing conditions over precursor structure in determining the nature of the pyrolysate has also been observed in earlier work by the authors on deposition of $CuME_2$ materials (M = In, Ga; E = S, Se) and as noted above, by O'Brien and coworkers in an elegant and rigorous study of nickel sulfide, selenide, and phosphide deposition from nickel dichalcogenoimidodiphosphinates $Ni((isopropyl)P(E)NP(E')(isopropyl))_2$ (E,E′ = S and/or Se).

Appendix—Full Structural Data for Compounds 1, 2a, 3, and 6

Tables XIII to XVI contain a more extensive list of bond lengths and angles than found in Table IV. Deposition numbers for crystallographic information files (CIFs) deposited with the Cambridge Crystallographic Data Centre (CCDC) are given in Table II. If desired, CIFs can be requested from CCDC.

TABLE XIII.—BOND LENGTHS AND ANGLES
FOR $Ni(S_2CN^iPrBz)_2$ **1**

Bond length, Å		Bond angle, deg	
Ni–S(21)	2.1993(5)	S(21)–Ni–S(12)	100.02(2)
Ni–S(12)	2.1999(5)	S(21)–Ni–S(22)	79.32(1)
Ni–S(22)	2.2055(5)	S(12)–Ni–S(22)	178.96(2)
Ni–S(11)	2.2111(5)	S(21)–Ni–S(11)	178.54(2)
S(11)–C(10)	1.722(1)	S(12)–Ni–S(11)	79.25(1)
S(12)–C(10)	1.722(1)	S(22)–Ni–S(11)	101.40(1)
S(21)–C(20)	1.728(1)	C(10)–S(11)–Ni	85.41(6)
S(22)–C(20)	1.722(1)	C(10)–S(12)–Ni	85.78(7)
N(1)–C(10)	1.318(2)	C(20)–S(21)–Ni	85.78(6)
N(2)–C(20)	1.319(2)	C(20)–S(22)–Ni	85.75(7)
N(1)–C(110)	1.470(2)	C(10)–N(1)–C(110)	120.0(1)
N(1)–C(122)	1.492(2)	C(10)–N(1)–C(122)	120.6(1)
N(2)–C(210)	1.475(2)	C(110)–N(1)–C(122)	118.5(1)
N(2)–C(222)	1.492(2)	C(20)–N(2)–C(210)	120.8(1)
C(110)–C(111)	1.512(3)	C(20)–N(2)–C(222)	119.8(1)
C(121)–C(122)	1.526(3)	C(210)–N(2)–C(222)	118.6(1)
C(122)–C(123)	1.516(3)	N(1)–C(10)–S(12)	124.6(1)
C(210)–C(211)	1.515(3)	N(1)–C(10)–S(11)	125.9(1)
C(221)–C(222)	1.523(3)	S(12)–C(10)–S(11)	109.5(1)
C(222)–C(223)	1.517(3)	N(2)–C(20)–S(22)	125.6(1)
C(111)–C(116)	1.379(3)	N(2)–C(20)–S(21)	125.3(1)
C(111)–C(112)	1.383(3)	S(22)–C(20)–S(21)	109.2(1)
C(112)–C(113)	1.388(3)	N(1)–C(110)–C(111)	115.3(1)
C(113)–C(114)	1.371(3)	C(116)–C(111)–C(112)	118.5(1)
C(114)–C(115)	1.373(3)	C(116)–C(111)–C(110)	123.5(1)
C(115)–C(116)	1.391(3)	C(112)–C(111)–C(110)	118.0(1)
C(211)–C(216)	1.393(3)	N(1)–C(122)–C(123)	111.3(1)
C(211)–C(212)	1.386(3)	N(1)–C(122)–C(121)	108.7(1)
C(212)–C(213)	1.393(3)	C(123)–C(122)–C(121)	113.0(1)
C(213)–C(214)	1.373(3)	N(2)–C(210)–C(211)	114.6(1)
C(214)–C(215)	1.378(3)	C(216)–C(211)–C(212)	118.7(1)
C(215)–C(216)	1.388(3)	C(216)–C(211)–C(210)	121.0(1)
----------	----------	C(212)–C(211)–C(210)	120.2(1)
----------	----------	N(2)–C(222)–C(223)	111.9(1)
----------	----------	N(2)–C(222)–C(221)	109.0(1)
----------	----------	C(223)–C(222)–C(221)	112.7(1)

TABLE XIV.—SELECT BOND LENGTHS AND ANGLES FOR $Ni(S_2CNEt^nBu)_2$ **2a**

Bond length, Å		Bond angle, deg	
Ni–S(1)	2.2072(6)	S(1)–Ni–S(1a)	180.00(2)
Ni–S(1a)	2.2073(6)	S(1)–Ni–S(2a)	100.72(2)
Ni–S(2)	2.2093(6)	S(1)–Ni–S(2)	79.28(2)
Ni–S(2a)	2.2094(6)	S(1a)–Ni–S(2a)	79.28(2)
S(1)–C(1)	1.723(3)	S(1a)–Ni–S(2)	100.72(2)
S(2)–C(1)	1.720(2)	S(2)–Ni–S(2a)	180.00(2)
C(1)–N(1)	1.321(3)	C(1)–S(1)–Ni	85.42(8)
N(1)–C(11)	1.470(3)	C(1)–S(2)–Ni	85.42(9)
N(1)–C(15)	1.472(3)	N(1)–C(1)–S(2)	125.0(1)
C(11)–C(12)	1.512(3)	N(1)–C(1)–S(1)	125.1(1)
C(12)–C(13)	1.526(3)	S(2)–C(1)–S(1)	109.9(1)
C(13)–C(14)	1.522(4)	C(1)–N(1)–C(11)	121.6(1)
C(15)–C(16)	1.523(4)	C(1)–N(1)–C(15)	121.3(2)
----------	----------	C(11)–N(1)–C(15)	117.1(2)
----------	----------	N(1)–C(11)–C(12)	112.3(2)
----------	----------	C(11)–C(12)–C(13)	112.0(2)
----------	----------	C(14)–C(13)–C(12)	113.2(2)
----------	----------	N(1)–C(15)–C(16)	111.5(2)

TABLE XV.—BOND LENGTHS AND ANGLES
FOR $Ni(S_2CNPhBz)_2$ **3**

Bond length, Å		Bond angle, deg	
Ni–S(1)	2.2005(5)	S(1)–Ni–S(1a)	180.000(1)
Ni–S(1a)	2.2005(5)	S(1)–Ni–S(2)	79.55(1)
Ni–S(2)	2.2035(4)	S(1)–Ni–S(2a)	100.45(1)
Ni–S(2a)	2.2035(4)	S(2)–Ni–S(2a)	180.00(1)
S(1)–C(1)	1.721(1)	C(1)–S(1)–Ni	85.21(6)
S(2)–C(1)	1.718(1)	C(1)–S(2)–Ni	85.19(6)
N(1a)–C(1a)	1.318(2)	C(1)–N(1)–C(11)	120.2(1)
N(1)–C(11)	1.445(2)	C(1)–N(1)–C(20)	122.1(1)
N(1)–C(20)	1.475(2)	C(11)–N(1)–C(20)	117.5(1)
C(1)–N(1)	1.318(2)	N(1)–C(1)–S(2)	124.8(1)
C(11)–C(12)	1.380(2)	N(1)–C(1)–S(1)	125.2(1)
C(11)–C(16)	1.382(2)	S(2)–C(1)–S(1)	110.04(9)
C(12)–C(13)	1.377(2)	C(12)–C(11)–C(16)	121.1(1)
C(13)–C(14)	1.374(3)	C(12)–C(11)–N(1)	118.9(1)
C(14)–C(15)	1.376(3)	C(16)–C(11)–N(1)	120.1(1)
C(15)–C(16)	1.393(2)	C(13)–C(12)–C(11)	119.7(1)
C(20)–C(21)	1.509(2)	C(14)–C(13)–C(12)	120.1(1)
C(21)–C(22)	1.373(3)	C(13)–C(14)–C(15)	120.2(1)
C(21)–C(26)	1.387(3)	C(14)–C(15)–C(16)	120.6(1)
C(22)–C(23)	1.392(3)	C(11)–C(16)–C(15)	118.4(1)
C(23)–C(24)	1.356(3)	N(1)–C(20)–C(21)	113.7(1)
C(24)–C(25)	1.370(3)	C(22)–C(21)–C(26)	118.2(1)
C(25)–C(26)	1.383(3)	C(22)–C(21)–C(20)	120.9(1)
----------	----------	C(26)–C(21)–C(20)	120.8(1)
----------	----------	C(21)–C(22)–C(23)	120.7(1)
----------	----------	C(24)–C(23)–C(22)	120.6(1)
----------	----------	C(23)–C(24)–C(25)	119.5(1)
----------	----------	C(24)–C(25)–C(26)	120.5(1)
----------	----------	C(25)–C(26)–C(21)	120.5(1)

TABLE XVI.—BOND LENGHTHS AND ANGLES
FOR Ni(PPh_3)($S_2CNPhBz$)Cl **6**

Bond length, Å		Bond angle, deg	
Ni–Cl	2.1800(8)	Cl–Ni–S(1)	171.01(3)
Ni–S(1)	2.1878(8)	Cl–Ni–P(2)	97.00(3)
Ni–P(2)	2.2010(8)	S(1)–Ni–P(2)	91.47(3)
Ni–S(2)	2.2342(8)	Cl–Ni–S(2)	93.12(3)
S(1)–C(10)	1.722(3)	S(1)–Ni–S(2)	78.31(3)
S(2)–C(10)	1.714(3)	P(2)–Ni–S(2)	169.64(3)
P(2)–C(231)	1.823(3)	C(10)–S(1)–Ni	87.1(1)
P(2)–C(221)	1.824(3)	C(10)–S(2)–Ni	85.8(1)
P(2)–C(211)	1.835(3)	C(231)–P(2)–C(221)	105.9(1)
N(10)–C(10)	1.313(4)	C(231)–P(2)–C(211)	104.1(1)
N(10)–C(111)	1.456(4)	C(221)–P(2)–C(211)	102.6(1)
N(10)–C(120)	1.478(3)	C(231)–P(2)–Ni	110.81(9)
C(111)–C(116)	1.364(4)	C(221)–P(2)–Ni	110.12(9)
C(111)–C(112)	1.373(4)	C(211)–P(2)–Ni	122.00(9)
C(112)–C(113)	1.383(4)	C(10)–N(10)–C(111)	121.1(2)
C(113)–C(114)	1.368(5)	C(10)–N(10)–C(120)	121.1(2)
C(114)–C(115)	1.374(4)	C(111)–N(10)–C(120)	117.8(2)
C(115)–C(116)	1.384(5)	N(10)–C(10)–S(2)	126.2(2)
C(120)–C(121)	1.510(4)	N(10)–C(20)–S(1)	125.1(2)
C(121)–C(126)	1.391(4)	S(2)–C(10)–S(1)	108.7(1)
C(121)–C(122)	1.389(4)	C(116)–C(111)–C(112)	121.1(3)
C(122)–C(123)	1.391(5)	C(116)–C(111)–N(10)	119.0(2)
C(123)–C(124)	1.382(6)	C(112)–C(111)–N(10)	119.9(3)
C(124)–C(125)	1.362(5)	N(10)–C(120)–C(121)	111.8(2)
C(125)–C(126)	1.382(4)	C(212)–C(211)–C(216)	118.7(2)
C(211)–C(216)	1.389(4)	C(212)–C(211)–P(2)	119.3(1)
C(211)–C(212)	1.385(4)	C(216)–C(211)–P(2)	121.8(2)
C(212)–C(213)	1.381(4)	C(222)–C(221)–C(226)	118.7(3)
C(213)–C(214)	1.391(4)	C(222)–C(221)–P(2)	121.8(2)
C(214)–C(215)	1.373(4)	C(226)–C(221)–P(2)	119.5(2)
C(215)–C(216)	1.391(4)	C(122)–C(121)–C(126)	118.9(3)
C(221)–C(226)	1.395(4)	C(122)–C(121)–C(120)	120.9(3)
C(223)–C(224)	1.386(4)	C(126)–C(121)–C(120)	120.2(3)
C(231)–C(236)	1.399(4)	C(232)–C(231)–C(236)	119.2(3)
C(233)–C(234)	1.378(4)	C(232)–C(231)–P(2)	122.9(2)
----------	----------	C(236)–C(231)–P(2)	117.8(2)

References

1. Thorn, G.D.; and Ludwig, R.A.: The Dithiocarbamates and Related Compounds. Elsevier Publishing, Amsterdam, 1962.
2. Coucouvanis, Dimitri: The Chemistry of the Dithioacid and 1,1-Dithiolate Complexes. Progress in Inorganic Chemistry, Stephen J. Lippard, ed., Vol. 11, John Wiley & Sons, Inc., New York, 1970, pp. 233–371.
3. Coucouvanis, Dimitri: The Chemistry of the Dithioacid and 1, 1-Dithiolate Complexes, 1968–1977. Progress in Inorganic Chemistry, Stephen J. Lippard, ed., Vol. 26, John Wiley & Sons, Inc., New York, 1979, pp. 301–469.
4. Heard, Peter J.: Main Group Dithiocarbamate Complexes. Progress in Inorganic Chemistry, Kenneth D. Karlin, ed., Vol. 53, John Wiley & Sons, Inc., Hoboken, NJ, 2005, pp. 1–70.
5. Hogarth, Graeme: Transition Metal Dithiocarbamates: 1978–2003. Progress in Inorganic Chemistry, Kenneth D. Karlin, ed., Vol. 53, John Wiley & Sons, Inc., Hoboken, NJ, 2005, pp. 71–561.
6. Fuentes-Martínez, Juan Pablo, et al.: Diorganotin(IV) Dithiocarbamate Complexes as Chromogenic Sensors of Anion Binding. Polyhedron, vol. 28, no. 18, 2009, pp. 3953–3966.
7. Cookson, James, et al.: Metal-Directed Assembly of Large Dinuclear Copper(II) Dithiocarbamate Macrocyclic Complexes. Inorg. Chim. Acta, vol. 363, no. 6, 2010, pp. 1195–1203.
8. Tlahuext, Hugo, et al.: Molecular Structures and Supramolecular Association of Chlorodiorganotin(IV) Complexes with Bis- and Tris-Dithiocarbamate Ligand. J. Organomet. Chem., vol. 696, 2011, pp. 693–701.
9. Wenclawiak, Bernd W., et al: Studies on Bulky Residual Group Substituted Arsenic(III) Dithiocarbamate Structures. Inorg. Chim. Acta, vol. 348, 2003, pp. 1–7.
10. Husain, Ahmad, et al.: Anagostic Interactions, Revisiting the Crystal Structure of Nickel Dithiocarbamate Complex and Its Antibacterial and Antifungal Studies. Polyhedron, vol. 30, no. 1, 2011, pp. 33–40.
11. Yan, Yan, et al.: Nickel(II) Dithiocarbamate Complexes Containing Sulforhodamine B as Fluorescent Probes for Selective Detection of Nitrogen Dioxide. J. Am. Chem. Soc., vol. 135, no. 14, 2013, pp. 5312–5315.
12. Rehman, Muneeb-Ur, et al.: Humidity-Sensing and DNA-Binding Ability of Bis(4-Benzylpiperazine-1-Carbodithioato-k^2 *S,S'*)Nickel(II). J. Coord. Chem., vol. 68, no. 2, 2015, pp. 295–307.
13. Hu, Jian-Qiang, et al.: Synergistic Antioxidation of Organic Molybdenum Complex With Dithiocarbamate Antioxidant Evaluated by Differential Scanning Calorimetry and Thin Film Micro Oxidation Test. Thermochim. Acta, vol. 453, no. 1, 2007, pp. 21–26.
14. Cui, Hua, et al.: Syntheses of Ni_3S_2, Co_9S_8, and ZnS by the Decomposition of Diethyldithiocarbamate Complexes. J. Solid State Chem., vol. 101, 1992, pp. 115–118.
15. Singhal, G.H., et al.: Formation of Transition Metal Sulfides by the Decomposition of Their Dithiolato Complexes. J. Solid State Chem., vol. 109, 1994, pp. 166–171.
16. Nomura, R., and Hyata, H.: Syntheses, Crystal Structure, Spectroscopic Characterization and Antifungal Activity of New N-R-Sulfonyldithiocarbamate Metal Complexes. Trans. Mater. Res. Soc. Jpn., vol. 26, 2001, p. 1283.
17. O'Brien, P.; and Park, J.H.; and Waters, J.: A Single Source Approach to Deposition of Nickel Sulfide Thin Films by LP–MOCVD. Thin Solid Films, vol. 431–432, 2003, pp. 502–505.
18. Hehemann, David G., et al.: Synthesis, Characterization and Decomposition Studies of Tris(*N,N*Dibenzyldithiocarbamato)Indium(III): Chemical Spray Deposition of Polycrystalline $CuInS_2$ on Copper Films. Mater. Sci. Eng. B, vol. 116, no. 3, 2005, pp. 381–389.
19. O'Brien, P.; and Waters, J.: Deposition of Ni and Pd Sulfide Thin Films via Aerosol-Assisted CVD. Chem. Vapor Depos., vol. 12, no. 10, 2006, pp. 620–626.
20. Nirmal, R. Max; Pandian, K.; and Sivakumar, K.: Cadmium (II) Pyrrolidine Dithiocarbamate Complex as Single Source Precursor for the Preparation of CdS Nanocrystals by Microwave Irradiation and Conventional Heating Process. Appl. Surf. Sci., vol. 257, no. 7, 2011, pp. 2745–2751.

21. Hollingsworth, Nathan, et al.: Active Nature of Primary Amines During Thermal Decomposition of Nickel Dithiocarbamates to Nickel Sulfide Nanoparticles. Chem. Mater., vol. 26, no. 21, 2014, pp. 6281–6292.
22. Prakasam, Balasubramaniam Arul, et al.: Synthesis, NMR Spectral and Single Crystal X-Ray Structural Studies on Ni(II) Dithiocarbamates. Fabrication of Nickel Sulfide Nanospheres by the Solvothermal Method. Polyhedron, vol. 81, 2014, pp. 588–596.
23. Prakasam, Balasubramaniam Arul, et al.: Spectral and Structural Studies on Ni(II) Dithiocarbamates: Nickel Sulfide Nanoparticles From a Dithiocarbamate Precursor. Inorg. Chim. Acta, vol. 425, 2015, pp. 239–246.
24. MacInnes, Andrew N., et al.: Enhancement of Photoluminescence Intensity of GaAs With Cubic GaS Chemical Vapor Deposited Using a Structurally Designed Single-Source Precursor. Appl. Phys. Lett., vol. 62, 1993, p. 711.
25. Hollingsworth, Jennifer A.; Hepp, Aloysius F.; and Buhro, William E.: Spray CVD of Copper Indium Sulfide Films: Control of Microstructure and Crystallographic Orientation. Chem. Vapor Depos., vol. 5, no. 3, 1999, pp. 105–108.
26. Banger, Kulbinder K.; Cowen, Jonathan; and Hepp, Aloysius F.: Synthesis and Characterization of the First Liquid Single-Source Precursors for the Deposition of Ternary Chalcopyrite ($CuInS_2$) Thin Film Materials. Chem. Mater., vol. 13, no. 11, 2001, pp. 3827–3829.
27. Banger, Kulbinder K., et al.: A New Facile Route for the Preparation of Single-Source Precursors for Bulk, Thin-Film, and Nanocrystallite I−III−VI Semiconductors. Inorg. Chem., vol. 42, no. 24, 2003, pp. 7713–7715.
28. Castro, Stephanie L., et al.: Synthesis and Characterization of Colloidal $CuInS_2$ Nanoparticles From a Molecular Single-Source Precursor. J. Phys. Chem. B, vol. 108, no. 33, 2004, pp. 12429–12435.
29. Hepp, Aloysius F., et al.: Spray CVD of Single-Source Precursors for Chalcopyrite I–III–VI2 Thin-Film Materials. Solution Processing of Inorganic Materials, David B. Mitzi, ed., John Wiley & Sons, Inc., Hoboken, NJ, 2009, pp. 157–198.
30. Masnovi, John, et al.: Structural Characterization of Copper-Indium Chalcopyrite Precursors $(PPh_3)_2CuIn(ER)_4$ [R = CH_3, E = S and R = Ph, E = S and Se]. Polyhedron, vol. 102, 2015, pp. 246–252.
31. Kullerud, G.; and Yund, R.A.: The Ni-S System and Related Minerals. J. Petrology, vol. 3, no. 1, 1962, pp. 126–175.
32. McWhan, D.B., et al.: Pressure-Temperature Phase Diagram and Crystal Structure of NiS. Phys. Rev. B, vol. 5, 1972, p. 2552.
33. Massalski, T.B., et al., eds.: Binary Alloy Phase Diagrams, 2nd Edition. ASM International, Materials Park, OH, 1990, pp. 2850–2853.
34. Stølen, Svein, et al.: Phase Stability and Structural Properties of $Ni_7S_{6\pm\delta}$S6 and Ni_9S_8 Heat Capacity and Thermodynamic Properties of Ni_7S_6 at Temperatures From 5 K to 970 K and of Ni_9S_8 at Temperatures From 5 K to 970 K and of Ni_9S_8 From 5 K to 673 K. J. Chem. Thermodyn., vol. 26, no. 9, 1994, pp. 987–1000.
35. Seim, Helene, et al.: Metastable Nickel Sulfides With Composition Close to Ni_7S_6—Stability and Structural Properties. J. Solid State Chem., vol. 121, no. 2, 1996, pp. 400–407.
36. Tilley, Richard D.; and Jefferson, David A.: The Synthesis of Nickel Sulfide Nanoparticles on Graphitized Carbon Supports. J. Phys. Chem. B, vol. 106, no. 42, 2002, pp. 10895–10901.
37. von Braun, J.: Zur Kenntniss der Thiuramdisulfide und Isothiuramdisulfide. I. Ber. Dtsch. Chem. Ges., vol. 35, no. 1, 1902, pp. 817–830.
38. Duffy, Norman V.: Ligand Exchange in Tris(Diorganodithiocarbamato)Iron(III) Complexes. Inorg. Chim. Acta, vol. 47, 1981, pp. 31–35.
39. Duffy, Norman V.; Movius, William G.; and Uhrich, David L.: Ligand Scrambling in the Preparation of Mixed Ligand Iron(III) Dithiocarbamates. Inorg. Chim. Acta, vol. 64, 1982, pp. L91–L93.
40. Otwinowski, Zbyszek; and Minor, Wladek: Processing of X-Ray Diffraction Data Collected in Oscillation Mode. Methods Enzymol., vol. 276, part A, 1997, pp. 307–326.

41. Beurskens, Paul, et al.: The DIRDIF-99 Program System. University of Nijmegen, The Netherlands, 1999.
42. Burla, M.C., et al.: SIR2004: An Improved Tool for Crystal Structure Determination and Refinement. J. Appl. Cryst., vol. 38, 2005, pp. 381–388.
43. Prince, E., ed.: International Tables of Crystallography. Vol. C, Third Ed., Wiley, New York, 2006.
44. Sheldrick, G.M.: A Short History of SHELX. Acta Cryst., vol. A64, 2008, pp. 112–122.
45. Burnett, Michael N.; and Johnson, Carroll K.: ORTEP–3: Oak Ridge Thermal Ellipsoid Plot Program for Crystal Structure Illustrations. ORNL–6895, 1996.
46. Motherwell, W.D.S.; and Clegg, W.: PLUTO. Program for Plotting Molecular and Crystal Structures. University of Cambridge, UK, 1978.
47. Shupack, S.I., et al.: The Electronic Structures of Square-Planar Metal Complexes. V. Spectral Properties of the Maleonitriledithiolate Complexes of Nickel, Palladium, and Platinum. J. Am. Chem. Soc., vol. 86, no. 21, 1964, pp. 4594–4602.
48. Dingle, R.: Electronic Spectrum of Crystalline Bis(Diethyldithiocarbamato)Nickel(II). Inorg. Chem., vol. 10, no. 6, 1971, pp. 1141–1144.
49. Vandebeek, Ronald R., et al.: Decomposition of Some Cyclic Dithiocarbamates. Canad. J. Chem., vol. 48, no. 14, 1970, pp. 2204–2209.
50. Mamba, Saul M., et al.: Spectral, Thermal and In Vitro Antimicrobial Studies of Cyclohexylamine-*N*-Dithiocarbamate Transition Metal Complexes. Spectrochim. Acta Mol. Biomol. Spectrosc., vol. 77, no. 3, 2010, pp. 579–587.
51. Kellner, Robert; Nikolov, George St.; and Trendafilova, Natasha: Detecting the Bonding Type of Dithiocarbamate Ligands in Their Complexes as Inferred From the Asymmetric CS Mode. Inorg. Chim. Acta, vol. 84, no. 2, 1984, pp. 233–239.
52. Shankaranarayana, M.L.; and Patel, C.C.: Infrared Absorption Studies on Some Derivatives of Xanthic, Dithiocarbamic and Trithiocarbonic Acids. Spectrochim. Acta, vol. 21, 1965, pp. 95–103.
53. Bonati, Flavio; and Ugo, Renato: Organotin(IV) N,N-Disubstituted Dithiocarbamates. J. Organomet. Chem., vol. 10, no. 2, 1967, pp. 257–268.
54. Coates, J.: Interpretation of Infrared Spectra, A Practical Approach. Encyclopedia of Analytical Chemistry, R.A. Meyers, ed., John Wiley & Sons, Ltd., Chichester, UK, 2000, pp. 10815–10837.
55. Hogarth, Graime, et al.: Functionalised Dithiocarbamate Complexes: Synthesis and Molecular Structures of Bis(2-Methoxyethyl)Dithiocarbamate Complexes $[M\{S_2CN(CH_2CH_2OMe)_2\}_2]$(M = Ni, Cu, Zn) and $[Cu\{S_2CN(CH_2CH_2OMe)_2\}_2][ClO_4]$. Inorg. Chim. Acta, vol. 362, no. 4, 2009, pp. 1361–1364.
56. Newman, P.W.G.; and White, A.H.: Crystal Structure of Bis(N-Methyldithiocarbamato)Nickel(II). J. Chem. Soc., Dalton Trans., 1972, pp. 1460–1463.
57. Kamenicek, Jiri, et al.: Determination of the Structure of Bis(Propyldithiocarbamate)Nickel(II). Collect. Czech. Chem. Commun., vol. 55, no. 4, 1990, pp. 1010–1014.
58. Halimehjani, Azim Ziyaei, et al.: Synthesis and Characterization of Transition Metal Dithiocarbamate Derivatives of 1-Aminoadamantane: Crystal Structure of (*N*-Adamantyldithiocarbamato)Nickel(II). Inorg. Chim. Acta, vol. 373, no. 1, 2011, pp. 282–285.
59. Martin, J.M., et al.: Crystal Structures of Bis-(N-Methyl-N-Phenyldithiocarbamato)-Nickel-(II) and -Copper(II). J. Chem. Soc., Dalton Trans., 1972, pp. 2233–2238.
60. Juhari, W.N.S. Wan, et al.: Bis(*N*-Butyl-*N*-Ethyldithiocarbamato-$\kappa^2 S,S'$)Nickel(II). Acta. Cryst., vol. E66, 2010, p. m339.
61. Cox, M.J.; and Tiekink, E.R.T.: The Crystal and Molecular Structures of Some Nickel(II)Bis(*O*-Alkyldithiocarbonate)s and Nickel(II)Bis(*N,N*-Dialkyldithiocarbamate)s: An Evaluation of the Coordination Potential of 1,1-Dithiolate Ligands in Their Nickel(II) Complexes. Z. Kristallogr., vol. 214, no. 4, 1999, pp. 242–250.
62. Beer, Paul D., et al.: Pyrrole-Based Metallo-Macrocycles and Cryptands. Dalton Trans., 2003, pp. 603–611.

63. Pastorek, Richard, et al.: Benzylisopropyldithiocarbamate Complexes of Nickel With Triphenylphosphine in the Coordination Sphere. Polyhedron, vol. 18, no. 22, 1999, pp. 2879–2883.
64. Pastorek, Richard, et al.: Ni(II) Benzylbutyldithiocarbamates Containing Monodentate Phosphines. J. Coord. Chem., vol. 60, no. 5, 2007, pp. 485–494.
65. Pastorek, Richard, et al.: Ni(II) Complexes of Unsymmetrical Phenyl and Phenethyl Dithiocarbamates and Triphenylphosphine. J. Coord. Chem., vol. 59, no. 4, 2006, pp. 437–444.
66. Pastorek, R., et al.: Dithiocarbamate Complexes of Nickel With Triphenylphosphine and Isothiocyanate as Mixed Ligands. Chemical Papers, vol. 48, no. 5, 1994, pp. 317–323.
67. Pastorek, Richard, et al.: Die Nickeldialkyldithiokarbamate Mit Triphenylphosphin. Acta Universitatis Palackianae Olomucensis Facultas Rerum Naturalium, Chemica XXXII, vol. 112, 1993, 7–18.
68. Pastorek, Richard, et al.: Pyrrolidinedithiocarbamate Complexes of Nickel With Phosphorus Donor Ligands in the Coordination Sphere. Polyhedron, vol. 15, no. 21, 1996, pp. 3691–3695.
69. Anderson, Gordon K.; and Cross, Ronald J.: Isomerisation Mechanisms of Square-Planar Complexes. Chem. Soc. Rev., vol. 9, 1980, pp. 182–215.
70. McWhan, D.B., et al.: Pressure-Temperature Phase Diagram and Crystal Structure of NiS. Phys. Rev. B, vol. 5, 1972, p. 2552.
71. Agrahari, Aditya, et al.: Structure and Conformation of *Meso*-2,4-di(*N*-Carbazolyl)Pentane. J. Mol. Struct., vol. 1076, 2014, pp. 183–187.
72. Cvek, Boris, et al.: Ni(II), Cu(II), and Zn(II) Diethyldithiocarbamate Complexes Show Various Activities Against the Proteasome in Breast Cancer Cells. J. Med. Chem., vol. 51, no. 2, 2008, pp. 6256–6258.
73. Masnovi, Michelle E., et al.: 9,10,12,13,14,15-Hexahydro-11*H*-9,10[1',3]Cyclopentanthracene in Two Modifications. J. Mol. Struct., vol. 1074, 2014, pp. 289–293.
74. Sengupta, S.K.; and Kumar, Shyam: Thermal Studies on Metal Dithiocarbamato Complexes. A Review. Thermochim. Acta, vol. 72, no. 3, 1984, pp. 349–361.
75. Sharma, Anand Kumar: Thermal Behaviour of Metal-Dithiocarbamates. Thermochim. Acta, vol. 104, 1986, pp. 339–372.
76. Gonçalves, N.S., et al.: Size-Strain Study of NiO Nanoparticles by X-Ray Powder Diffraction Line Broadening. Mater. Lett., vol. 72, 2012, pp. 36–38.
77. Chauhan, Ratna, et al.: 1,2-Bis(Diphenylphosphino)Ethane Nickel(II)Dithiocarbamate as Potential Precursor for Nickel Sulfide: Effect of Counter Anion on Phase and Morphology. Inorg. Chim. Acta, vol. 415, 2014, pp. 69–74.
78. Cavalheiro, Éder T.G., et al.: Correlation Between I.R. Spectra and Thermal Decomposition of Cobalt(II), Nickel(II), Copper(II) and Mercury(II) Complexes With Piperidinedithiocarbamate and Pyrrolidinedithiocarbamate. Trans. Met. Chem., vol. 25, no. 1, 2000, pp. 69–72.
79. Riekkola, M.L.; and Makitie, O.: Thermal Properties of Some Metal Chelates of Di-isobutyldithiocarbamic Acid. J. Therm. Anal., vol. 25, no, 1, 1982, pp. 89–94.
80. Pastorek, R., et al.: Die Nickelpyrrolidindithiokarbamate. Acta Universitatis Palackianae Olomucensis Facultas Rerum Naturalium, Chemica XXXIII, vol. 117, 1994, pp. 11–15.
81. Schierloh, E.M., et al.: Thermal Decomposition Pathways for Indium(III) and Gallium(III) Dithiocarbamates Derived From Primary Amines II. Thermogravimetric Analysis and Infrared Spectra. J. Undergrad. Chem. Res., vol. 10, no. 4, 2011, p. 123.
82. Pawloski, Gary A.: Quantitative Determination of Mineral Content of Geological Samples by X-Ray Diffraction. Am. Mineral., vol. 70, 1985, p. 663.
83. Davis, Briant L.; and Pawlowski, Gayle A.: Quantitative Determination of Mineral Content of Geological Samples by X-Ray Diffraction; Discussion and Reply. Am. Mineral., vol. 72, 1987, p. 438.

84. Patterson, A.L.: The Scherrer Formula for X-Ray Particle Size Determination. Phys. Rev., vol. 56, 1939, p. 978.
85. Bowen, P.: Particle Size Distribution Measurement From Millimeters to Nanometers and From Rods to Platelets. J. Disper. Sci. Tech., vol. 23, no. 5, 2002, pp. 631–662.
86. Panneerselvam, Arunkumar, et al.: Factors Controlling Material Deposition in the CVD of Nickel Sulfides, Selenides or Phosphides From Dichalcogenoimidodiphosphinato Complexes: Deposition, Spectroscopic and Computational Studies. Dalton Trans., vol. 39, 2010, pp. 6080–6091.